

***SMAI-JCM***  
SMAI JOURNAL OF  
COMPUTATIONAL MATHEMATICS

Shape optimisation with the level  
set method for contact problems in  
linearised elasticity

AYMERIC MAURY, GRÉGOIRE ALLAIRE & FRANÇOIS JOUVE  
Volume 3 (2017), p. 249-292.

<[http://smai-jcm.cedram.org/item?id=SMAI-JCM\\_2017\\_\\_3\\_\\_249\\_0](http://smai-jcm.cedram.org/item?id=SMAI-JCM_2017__3__249_0)>

© Société de Mathématiques Appliquées et Industrielles, 2017  
*Certains* droits réservés.

cedram

Article mis en ligne dans le cadre du  
Centre de diffusion des revues académiques de mathématiques  
<http://www.cedram.org/>





# Shape optimisation with the level set method for contact problems in linearised elasticity

AYMERIC MAURY<sup>1</sup>  
GRÉGOIRE ALLAIRE<sup>2</sup>  
FRANÇOIS JOUVE<sup>3</sup>

<sup>1</sup> Laboratoire J.L. Lions (UMR CNRS 7598), University Paris Diderot, Paris, France

*E-mail address:* amaury@cmap.polytechnique.fr

<sup>2</sup> CMAP (UMR CNRS 7641), Ecole Polytechnique, Palaiseau, France

*E-mail address:* gregoire.allaire@polytechnique.fr

<sup>3</sup> Laboratoire J.L. Lions (UMR CNRS 7598), University Paris Diderot, Paris, France

*E-mail address:* jouve@ljl.univ-paris-diderot.fr.

**Abstract.** This article is devoted to shape optimisation of contact problems in linearised elasticity, thanks to the level set method. We circumvent the shape non-differentiability, due to the contact boundary conditions, by using penalised and regularised versions of the mechanical problem. This approach is applied to five different contact models: the frictionless model, the Tresca model, the Coulomb model, the normal compliance model and the Norton-Hoff model. We consider two types of optimisation problems in our applications: first, we minimise volume under a compliance constraint, second, we optimise the normal force, with a volume constraint, which is useful to design compliant mechanisms. To illustrate the validity of the method, 2D and 3D examples are performed, the 3D examples being computed with an industrial software.

**Math. classification.** 74P05, 75P10, 74P15, 74M10, 74M15, 49Q10, 49Q12, 35J85.

**Keywords.** Shape and topology Optimisation; Level set method; Unilateral contact problems; Frictional contact; Penalisation and Regularisation.

## 1. Introduction

We study the shape optimisation of a structure, the behaviour of which is modelled by the equations of linearised elasticity with unilateral contact boundary conditions and friction conditions. From an industrial point of view, these kinds of boundary conditions are of great interest, as they enable a more detailed and accurate modelling of boundary conditions, compared to clamped or Dirichlet boundary conditions. From a mathematical point of view, they tend to make the whole optimisation more intricate. Indeed the mechanical problem takes the form of a variational inequality and, thus, is highly non-linear. The study of the existence and uniqueness of a solution for frictionless contact and its regularity were performed, for instance, in [15], [9], more recently in [4], [5] and, thanks to the use of pseudo-differential operators, in [54]. Similar results on frictionless auto-contact and auto-contact with Tresca friction can also be found in [40]. However, as soon as a more realistic friction model is taken into consideration, results on existence and uniqueness become harder to obtain [16], [38].

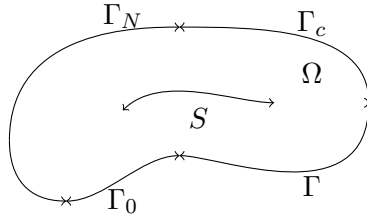
On the other hand, the shape optimisation of such problems presents the same difficulties as encountered in control theory of variational inequalities. As pointed out in [44] and [58], the frictionless contact solution can be written under the form of a projection onto a convex set, which is not differentiable in the usual sense but merely admits a so-called conical derivative [44]. Nevertheless, Mignot [44] managed to derive optimality conditions, thanks to this weak notion of differentiability. Using the conical derivative and writing the problem under a discretised form, Kocvara and al. [50] used a bundle algorithm to perform shape optimisation. Another way to get optimality conditions, see [6] and [3], is to introduce a regularised problem, depending on a small regularisation parameter, study its optimality conditions and pass to the limit when the regularisation parameter tends to zero. This approach,

called penalisation, was used in various numerical shape optimisation works: for example, with the SIMP method in [13], or with parameterised shapes (using splines) in [52] and [35]. Its convergence to the exact solution was proved in [14]. Another similar approach is the regularisation of the unilateral boundary conditions which was used in [60] and [59] in the context of the SIMP method. Some authors, as in [62] and [32], write a saddle point formulation of the problem and use the so-called Lagrangian method, ignoring the non-differentiability of the Lagrange multipliers arising in this formulation. We also point out the method which consists, first, to discretise the problem (without regularisation or penalisation) and, then, to perform shape optimisation on the discretised formulation, as in [29] where the contact boundary is optimised by moving the nodes of a finite element mesh. Of course, it is possible to perform optimisation without derivatives, as in [11] or [42], using genetic algorithms, but the price to pay is the very large number of required iterations. As far as theoretical results are concerned, we refer to [25], [26], [22], [24] and [27] where, for a particular optimisation problem, existence of an optimum is proved under assumptions of uniform Lipschitz regularity of the boundary, first proving the result for a discretisation, then passing to the continuous limit. Note that in [27], the penalised problem is studied for frictionless contact and the solution of a particular shape optimisation problem is proved to converge to the solution of the non-penalised problem. In these last articles, the contact boundary is meant to be optimised and so is parametrised thanks to a Lipschitz function. Some numerical experiments are provided where the contact boundary is optimised by moving the nodes of a finite element mesh.

When friction comes into play, the shape differentiation becomes even more difficult. In [58], for the Tresca model (also called the prescribed friction model), a conical derivative is computed, merely in two-space dimensions and for specific directions of differentiation. Once again, penalised and regularised formulations can be used as in [34], [3] and [61]. Theoretical results are also given for normal compliance model in [38] and [39] and for Coulomb friction model in [23]. For this last model of friction, the uniqueness of the contact solution is not ensured for the continuous model and examples of non-uniqueness can be built. Consequently, in [7] and [8], the authors analyse the derivation of the discretised problem, which admits a unique solution for small friction coefficients, by using subgradient calculus. Eventually, a thorough review of other results in shape optimisation for contact problems can be found in [31].

The goal of this paper is to apply the level set method for shape and topology optimisation [2] to contact problems, possibly including friction. To the best of our knowledge, this is the first time that this method is used for shape optimisation of contact problems. We investigate four types of friction, one of them being the Norton Hoff model which has not been previously used in shape optimisation. To easily compute shape derivatives and avoid the intricate notion of conical derivatives we rely on the classical idea of penalised and regularised formulations. We do not restrict ourselves to simple objective functions like compliance but also consider more involved ones, depending on the normal force. Examples of such criteria depending on the normal force can be found in [37] and [11] but we choose to build different ones, more adapted to our needs. Objective functions depending on the normal force are useful to design compliant mechanisms, for example. Note that, if the purpose of this article is to apply the level set method to several different contact behaviours and different objective functions, it is not to optimise the contact boundaries (as in many previous works) but rather the other parts of the structural boundary.

Section 2 presents the frictionless contact model and gives four different friction conditions depending on the chosen model: Tresca, Coulomb, Norton Hoff and normal compliance model. For each of them, we recall an existence result for its solution. Section 3 focuses on how to regularise these problems in order to easily compute derivatives of their solutions with respect to the shape. We choose to penalise the normal condition and to regularise the tangential ones which will enable us to compute shape derivatives. The section ends with a short analysis of existence results of these new formulations. In Section 4, a general shape optimisation problem is introduced and shape derivatives are calculated


 FIGURE 2.1. The open set  $\Omega$  and its boundaries.

using the adjoint method. Criteria used for the numerical examples are also proposed, especially criteria depending on the normal force. Section 5 briefly recalls the main ideas of the level set method for shape optimisation. Our numerical results are collected in Section 6. A large range of examples shows the good performances of our approach. We did not observe a high sensitivity of the optimised solutions to the regularisation and penalisation parameters. The 2D cases are performed with the Scilab free software [55], while the 3D examples are computed using the finite element software SYSTUS from ESI-Group [17]. Eventually we conclude and give some perspectives in Section 7.

## 2. Contact models in linearised elasticity

In this paper  $\Omega$  denotes an open bounded subset of  $\mathbb{R}^d$  where  $d = 2$  or  $3$  and represents the shape of the structure we want to optimise. Its boundary is divided into five disjoint parts, meaning that:

$$\partial\Omega = \Gamma_0 \cup \Gamma_N \cup \Gamma_c \cup \Gamma \cup S.$$

The structure  $\Omega$  is full of a linear isotropic elastic material with a Hooke's law characterised by  $A$ , for any  $\tau$  symmetric matrix, as:

$$A\tau = 2\mu\tau + \lambda\text{Tr}(\tau)I_d$$

where  $\mu$  and  $\lambda$  are the Lamé moduli. On  $\Gamma_0$ , the structure is clamped and on  $\Gamma_N$  a force is applied. The free part of the boundary is  $\Gamma$  and the parts where contact conditions are enforced are  $S$  and  $\Gamma_c$ .  $\Gamma_c$  models a contact with an undeformable body, whereas  $S$  is an auto-contact part (as for instance a crack could be). So  $S$  lies in the interior of  $\bar{\Omega}$ , see Figure 2.1. We assume that  $\Omega \cup S$  is smooth, as well as the partition of its boundary, and that  $\Gamma_0$  is of non-zero surface measure (so that Poincaré and Korn inequalities hold true).

The displacement field  $u$  is then solution of the linearised elasticity system:

$$\begin{cases} -\text{div}(Ae(u)) & = f & \text{in } \Omega \\ u & = 0 & \text{on } \Gamma_0 \\ Ae(u)n & = g & \text{on } \Gamma_N \\ Ae(u)n & = 0 & \text{on } \Gamma \end{cases} \quad (2.1)$$

complemented with contact boundary conditions on  $\Gamma_c$  and  $S$ , which depend on the type of contact model we use. In (2.1),  $n$  denotes the exterior unit normal,  $e(u) = (\nabla u + (\nabla u)^T)/2$  is the strain tensor and  $Ae(u)$  is the stress tensor. To specify the contact boundary conditions, we first introduce some notations. For a vector  $v \in \mathbb{R}^d$ , we denote by  $v_t$  its tangential part:

$$v_t = v - (v \cdot n)n.$$

We also note the jump through  $S$  of  $v$ , noting  $S_-$  and  $S_+$  the two sides of  $S$ :

$$[v] = v|_{S_-} - v|_{S_+}.$$

## 2.1. Sliding Contact

Sliding contact assumes there is no friction, which means that  $(Ae(u)n)_t = 0$  on  $\Gamma_c$  and  $(Ae(u)n)_t = 0$  on  $S_-$  and  $S_+$ . For the normal part on  $\Gamma_c$ , three conditions are needed:

$$u \cdot n \leq 0 \quad (2.2)$$

which prevents the penetration,

$$Ae(u)n \cdot n \leq 0 \quad (2.3)$$

meaning that the normal force on the contact surface is always in the opposite sense to the outward normal and the complementarity condition

$$(u \cdot n)(Ae(u)n \cdot n) = 0 \quad (2.4)$$

imposes either a contact:  $(u \cdot n) = 0$  or, when there is no contact, a no force condition on  $\Gamma_c$ :  $(Ae(u)n \cdot n) = 0$ .

Concerning the normal part on  $S$ , the conditions are similar in terms of jumps:

$$\begin{cases} [u] \cdot n_- \leq 0 \\ Ae(u|_{S_-})n_- \cdot n_- = Ae(u|_{S_+})n_- \cdot n_- \leq 0 \\ ([u] \cdot n_-)(Ae(u|_{S_-})n_- \cdot n_-) = 0, \end{cases} \quad (2.5)$$

where  $n_-$  is the normal to  $S_-$  pointing toward  $S_+$ .

Coupling these boundary conditions with (2.1), the sliding contact problem can be written as:

$$\left\{ \begin{array}{ll} -\operatorname{div}(Ae(u)) = f & \text{in } \Omega \\ u = 0 & \text{on } \Gamma_0 \\ Ae(u)n = g & \text{on } \Gamma_N \\ Ae(u)n = 0 & \text{on } \Gamma \\ u \cdot n \leq 0 & \text{on } \Gamma_c \\ Ae(u)n \cdot n \leq 0 & \text{on } \Gamma_c \\ (u \cdot n)(Ae(u)n \cdot n) = 0 & \text{on } \Gamma_c \\ [u] \cdot n_- \leq 0 & \text{on } S \\ Ae(u|_{S_-})n_- \cdot n_- = Ae(u|_{S_+})n_- \cdot n_- \leq 0 & \text{on } S \\ ([u] \cdot n_-)(Ae(u|_{S_-})n_- \cdot n_-) = 0 & \text{on } S \\ (Ae(u)n)_t = 0 & \text{on } \Gamma_c \cup S. \end{array} \right. \quad (2.6)$$

Problem (2.6) can also be written as a variational inequality [15], where

$$K(\Omega) = \left\{ v \in H_{\Gamma_0}^1(\Omega)^d, v \cdot n \leq 0 \text{ on } \Gamma_c, [v] \cdot n_- \leq 0 \text{ on } S \right\}$$

is a closed convex set and  $H_{\Gamma_0}^1(\Omega)^d = \left\{ v \in (H^1(\Omega))^d, v = 0 \text{ on } \Gamma_0 \right\}$ :

find  $u \in K(\Omega)$  such that

$$\int_{\Omega} Ae(u) : e(v - u) dx \geq \int_{\Omega} f \cdot (v - u) dx + \int_{\Gamma_N} g \cdot (v - u) ds \quad \forall v \in K(\Omega) \quad (2.7)$$

with  $f \in L^2(\Omega)^d$  and  $g \in L^2(\Gamma_N)^d$ .

From (2.7) it follows that (2.6) is the Euler-Lagrange optimality condition of the minimisation problem:

$$u = \operatorname{argmin}_{v \in K(\Omega)} \frac{1}{2} \int_{\Omega} Ae(v) : e(v) dx - \int_{\Omega} f \cdot v dx - \int_{\Gamma_N} g \cdot v ds \quad (2.8)$$

which will be useful in the next section to penalise the problem.

The proof of existence and uniqueness of the solution  $u$  to (2.8) or (2.6) is a direct consequence of theorem 2.1 in [36] and Korn inequality (theorem 1.2.1 in [16] and theorem 3.1 in chapter 3 of [15]). It relies on the convexity of both  $K(\Omega)$  and the quadratic energy functional.

## 2.2. Contact with friction

To add some friction conditions, it is necessary to change the tangential condition  $(Ae(u)n)_t = 0$  on  $\Gamma_c$  and  $S$ . The most popular friction model is the Coulomb one, but we first state a simpler model derived from it and then present the different models which will be used in the shape optimisation part.

### 2.2.1. Tresca model

The Tresca friction model, also known as the model of given friction, was introduced in [15]. Even if it does not represent a realistic mechanical model, it can be used numerically to obtain the solution of the Coulomb friction model in a fixed point method and is mathematically well-posed. For the normal part (2.2), (2.3), (2.4) and (2.5) are kept. For the tangential part on  $\Gamma_c$  it is stated as:

$$\begin{aligned} \|(Ae(u)n)_t\| &\leq \sigma_{\text{tr}} && \text{on } \Gamma_c \\ \|(Ae(u)n)_t\| &< \sigma_{\text{tr}} \Rightarrow u_t = 0 && \text{on } \Gamma_c \\ \|(Ae(u)n)_t\| &= \sigma_{\text{tr}} \Rightarrow \exists \lambda \geq 0, u_t = -\lambda(Ae(u)n)_t && \text{on } \Gamma_c \end{aligned} \quad (2.9)$$

and on  $S$ :

$$\begin{aligned} (Ae(u)n)_t &= (Ae(u|_{S_-})n_-)_t = -(Ae(u|_{S_+})n_+)_t && \text{on } S \\ \|(Ae(u)n)_t\| &\leq \sigma_{\text{tr}} && \text{on } S \\ \|(Ae(u)n)_t\| &< \sigma_{\text{tr}} \Rightarrow [u_t] = 0 && \text{on } S \\ \|(Ae(u)n)_t\| &= \sigma_{\text{tr}} \Rightarrow \exists \lambda \geq 0, [u_t] = -\lambda(Ae(u|_{S_-})n_-)_t && \text{on } S \end{aligned}$$

where  $\|\cdot\|$  denotes the classical euclidian norm on  $\mathbb{R}^d$  and  $\sigma_{\text{tr}}$  is a smooth function representing the coefficient of friction. When the tangential force is smaller than the coefficient of friction, there is no sliding. If the tangential force reaches the threshold  $\sigma_{\text{tr}}$ , sliding can appear. This model is not well-suited to represent real phenomena, since the tangential force does not take into account the normal force. Yet, like the problem (2.6), (2.9) can be written as a variational inequality and a minimisation problem of respectively the form: find  $u \in K(\Omega)$  such that

$$\int_{\Omega} Ae(u) : e(v - u) dx + j_{\text{tr}}(v) - j_{\text{tr}}(u) \geq \int_{\Omega} f \cdot (v - u) dx + \int_{\Gamma_N} g \cdot (v - u) ds \quad \forall v \in K(\Omega) \quad (2.10)$$

and

$$u = \operatorname{argmin}_{v \in K(\Omega)} \frac{1}{2} \int_{\Omega} Ae(v) : e(v) dx - \int_{\Omega} f \cdot v dx - \int_{\Gamma_N} g \cdot v ds + j_{\text{tr}}(v) \quad (2.11)$$

with

$$j_{\text{tr}}(v) = \int_{\Gamma_c} \sigma_{\text{tr}} \|v_t\| ds + \int_S \sigma_{\text{tr}} \|[v]_t\| ds.$$

The proof of existence and uniqueness of the solution  $u$  of (2.11) is given in theorem 1.5.2 of [16]. Once again it relies on the convexity of the minimised functional.

### 2.2.2. Coulomb friction

The model of Coulomb friction is similar to the Tresca one, changing  $\sigma_{tr}$  into  $\mu$ , a friction coefficient, times the norm of the normal force. For  $\Gamma_c$ :

$$\begin{aligned} \|(Ae(u)n)_t\| &\leq \mu|(Ae(u)n \cdot n)| && \text{on } \Gamma_c \\ \|(Ae(u)n)_t\| &< \mu|(Ae(u)n \cdot n)| \Rightarrow u_t = 0 && \text{on } \Gamma_c \\ \|(Ae(u)n)_t\| &= \mu|(Ae(u)n \cdot n)| \Rightarrow \exists \lambda \geq 0, u_t = -\lambda(Ae(u)n)_t && \text{on } \Gamma_c \end{aligned}$$

and for  $S$ :

$$\begin{aligned} (Ae(u)n)_t &= (Ae(u|_{S_-})n_-)_t = -(Ae(u|_{S_+})n_+)_t && \text{on } S \\ \|(Ae(u)n)_t\| &\leq \mu|(Ae(u)n \cdot n)| && \text{on } S \\ \|(Ae(u)n)_t\| &< \mu|(Ae(u)n \cdot n)| \Rightarrow [u_t] = 0 && \text{on } S \\ \|(Ae(u)n)_t\| &= \mu|(Ae(u)n \cdot n)| \Rightarrow \exists \lambda \geq 0, [u_t] = -\lambda(Ae(u|_{S_-})n_-)_t && \text{on } S. \end{aligned}$$

For the normal part there is no change in the boundary conditions: (2.2), (2.3), (2.4) and (2.5). This can be written as the following variational inequality: find  $u \in K(\Omega)$  such that

$$\int_{\Omega} Ae(u) : e(v - u) dx + j_{co}(u, v) - j_{co}(u, u) \geq \int_{\Omega} f \cdot (v - u) dx + \int_{\Gamma_N} g \cdot (v - u) ds \quad \forall v \in K(\Omega) \quad (2.12)$$

with

$$j_{co}(u, v) = \int_{\Gamma_c} \mu|(Ae(u)n \cdot n)| \|v_t\| ds + \int_S \mu|(Ae(u)n \cdot n)| \|[v]_t\| ds.$$

which is a function of two variables.

This model is studied in chapters 1 and 3 of [16]. It is not equivalent to a minimisation problem. To our knowledge, there is no uniqueness results for this problem and the existence is only ensured for small friction coefficients. Yet the uniqueness was proven for the discretised problem in [21]. It is interesting, both for numerical [41] and theoretical [16] reasons, to note that this problem can be seen as the solution of a fixed point problem involving the solution of the Tresca model.

### 2.2.3. Norton-Hoff model

The Norton-Hoff model [45] is a variation of the previous friction model. The boundary condition is now a one-to-one relation between the tangential force and the tangential jump of the displacement (notwithstanding the normal force). It can be written as:

$$\begin{aligned} (Ae(u)n)_t &= \mu|(Ae(u)n \cdot n)| \|u_t\|^{\rho-1} u_t && \text{on } \Gamma_c \\ (Ae(u|_{S_-})n)_t &= -(Ae(u|_{S_+})n)_t = -\mu|(Ae(u)n \cdot n)| \|[u_t]\|^{\rho-1} [u_t] && \text{on } S \end{aligned} \quad (2.13)$$

where  $0 < \rho < 1$ . Adding the other boundary conditions (2.2), (2.3), (2.4) and (2.5), we obtain the following variational inequality. Find  $u \in K(\Omega)$  such that

$$\int_{\Omega} Ae(u) : e(v - u) dx + j_{nh}(u, v - u) \geq \int_{\Omega} f \cdot (v - u) dx + \int_{\Gamma_N} g \cdot (v - u) ds \quad \forall v \in K(\Omega) \quad (2.14)$$

where  $j_{nh}$  is a function of two variables, defined by

$$j_{nh}(u, v) = \int_{\Gamma_c} \mu|(Ae(u)n \cdot n)| \|u_t\|^{\rho-1} u_t \cdot v_t ds + \int_S \mu|(Ae(u)n \cdot n)| \|[u_t]\|^{\rho-1} [u_t] \cdot [v]_t ds.$$

The one-to-one relation mentioned in (2.13) makes the model numerically simpler to solve than the Coulomb one. Let us remark that (2.14) is not equivalent to a minimisation problem.

### 2.2.4. Normal compliance model

The last friction model considered is the normal compliance model presented in [47] and studied in [38]. It is pretty similar to a problem where the normal inequality constraint is penalised with a small penalisation coefficient. On  $\Gamma_c$  it takes the following form:

$$\begin{aligned}
 (Ae(u)n \cdot n)n &= -C_N(u \cdot n)_+^{m_N} n && \text{on } \Gamma_c \\
 \|(Ae(u)n)_t\| &\leq C_T(u \cdot n)_+^{m_T} && \text{on } \Gamma_c \\
 \|(Ae(u)n)_t\| < C_T(u \cdot n)_+^{m_T} &\Rightarrow u_t = 0 && \text{on } \Gamma_c \\
 \|(Ae(u)n)_t\| = C_T(u \cdot n)_+^{m_T} &\Rightarrow \exists \lambda \geq 0, u_t = -\lambda(Ae(u)n)_t && \text{on } \Gamma_c
 \end{aligned} \tag{2.15}$$

and on  $S$ :

$$\begin{aligned}
 (Ae(u|_{S_-})n \cdot n)n_- &= -(Ae(u|_{S_+})n \cdot n)n_- = -C_N([u] \cdot n_-)_+^{m_N} n && \text{on } S \\
 (Ae(u)n)_t &= (Ae(u|_{S_-})n_-)_t = -(Ae(u|_{S_+})n_+)_t && \text{on } S \\
 \|(Ae(u)n)_t\| &\leq C_T([u] \cdot n_-)_+^{m_T} && \text{on } S \\
 \|(Ae(u)n)_t\| < C_T([u] \cdot n_-)_+^{m_T} &\Rightarrow [u_t] = 0 && \text{on } S \\
 \|(Ae(u)n)_t\| = C_T([u] \cdot n_-)_+^{m_T} &\Rightarrow \exists \lambda \geq 0, [u_t] = -\lambda(Ae(u|_{S_-})n_-)_t && \text{on } S
 \end{aligned}$$

where  $(\cdot)_+ = \max(0, \cdot)$ ,  $C_N$  and  $C_T$  are material coefficients and  $m_N$  and  $m_T$  are typically equal to 1 or 2 (see [38] for the possible value depending on the dimension  $d$ ). Contrary to the other friction models, the normal part is different from the case of sliding contact. Again, it is possible to write a variational inequality equivalent to (2.15). Find  $u \in K(\Omega)$  such that, for any  $v \in H_{\Gamma_0}^1(\Omega)^d$ ,

$$\int_{\Omega} Ae(u) : e(v - u) dx + j_{N,nc}(u, v - u) + j_{T,nc}(u, v) - j_{T,nc}(u, u) \geq \int_{\Omega} f \cdot (v - u) dx + \int_{\Gamma_N} g \cdot (v - u) ds, \tag{2.16}$$

where

$$\begin{aligned}
 j_{N,nc}(u, v) &= \int_{\Gamma_c} C_N(u \cdot n)_+^{m_N} v \cdot n ds + \int_S C_N([u] \cdot n_-)_+^{m_N} [v] \cdot n ds, \\
 j_{T,nc}(u, v) &= \int_{\Gamma_c} C_T(u \cdot n)_+^{m_T} \|v_t\| ds + \int_S C_T([u] \cdot n_-)_+^{m_T} \|[v]_t\| ds.
 \end{aligned}$$

This model allows interpenetration, which can represent a material loss at the surface of the material in contact. Existence and uniqueness results are given and discussed in [38] and [30] under smallness conditions on the coefficients  $C_N$  and  $C_T$ . Here again (2.16) is not equivalent to a minimisation problem.

## 3. Penalised and regularised formulations

As our goal is to optimise, thanks to a gradient algorithm, and therefore to compute the derivative of some cost functions depending on the displacement  $u$ , we need to investigate the differentiability properties of  $u$  with respect to the shape. Based on the work of [44], the authors of [58] have shown that the solution  $u$  of (2.7) admits at most a conical derivative because of the non-differentiability of the projection map on closed convex sets in Hilbert spaces. We shall not define precisely what is a conical derivative (a type of "weak" multi-valued directional derivative). Let us simply say that it is quite difficult to use it in numerical practice since it requires a subgradient optimisation algorithm (see [50], for example, in finite dimension).

To avoid such intricate optimisation techniques, let us quickly investigate the different ways to numerically compute the solutions of problems described in Section 2. According to [18], there exist two main methods: the Lagrangian method and the penalisation method. The Lagrangian method

Name	Classical Equations	Penalised and Regularised equations
Frictionless	(2.7)-(2.8)	(3.3)
Tresca	(2.10)-(2.11)	(3.4)
Coulomb	(2.12)	(3.5)
Norton-Hoff	(2.14)	(3.6)
Normal compliance	(2.16)	(3.7)

TABLE 3.1. Correspondences between the classical contact equations and their associated penalised and regularised ones in the present paper.

introduces a Lagrange multiplier for the contact constraint, which will not be differentiable (basically for the same reasons preventing the solution  $u$  from being differentiable). It leads to a forward problem with complementarity constraints and hence to a shape optimisation problem which has to be solved by a mathematical programming algorithm with complementarity constraints. On the other hand, the penalisation method has the nice property to transform inequalities into equations and thus changes projection on closed convex sets into projection on linear spaces (in our cases  $H_{\Gamma_0}^1(\Omega)$ ). In particular, for this penalisation approach, it is possible to differentiate these new equations. Consequently, we choose to study and use these penalised formulations.

In the different contact problems presented, there are two kinds of reasons which trigger the appearance of inequalities. The first one, concerning the normal component of  $u$  on the boundary, is that  $u$  belongs to a convex set. This constraint will be penalised. The second one is the singularity in the tangential friction formulation due to the presence of the norm  $\|\cdot\|$  which is not differentiable at zero. This term will be regularised, thanks to a regularisation of the norm  $\|\cdot\|$ . Table 3.1 lists the correspondences between the classical contact equations (presented in the previous section) and their associated penalised and regularised ones which are established below.

### 3.1. Penalisation for the convex set

We now present the penalisation used to get rid of the constraint stating that the solution  $u$  is required to belong to  $K(\Omega)$ . This penalisation will be used for every model but the normal compliance one, and we explain how to add it to change the inequalities into equations or other inequalities. As a matter of fact, for problems involving friction, to get equations we also need to regularise the friction term (as said before). This is the reason why we only write the penalised equation associated with (2.11) in this subsection. For other models, they can be found in the next one.

To add the penalisation, the procedure differs whether the initial problem can be written as a minimisation problem, (2.11) and (2.8), or not, (2.12) and (2.14).

For (2.11) and (2.8), we change the functional to be minimised and the set of admissible solutions. Instead of minimising on  $K(\Omega)$ , we minimise on  $H_{\Gamma_0}^1(\Omega)^d$ . To approximate the condition  $v \cdot n \leq 0$  on  $\Gamma_c$  and  $[v] \cdot n_- \leq 0$  on  $S$ , we add to the functional a term of the form:

$$j_{N,\epsilon}(u) = \frac{1}{\epsilon} \left( \int_{\Gamma_c} \int_0^{u \cdot n} \phi_\eta(t) dt ds + \int_S \int_0^{[u] \cdot n} \phi_\eta(t) dt ds \right) \quad (3.1)$$

where  $\phi_\eta$  is a smooth function (at least  $C^1$ ) meant to regularise  $t \rightarrow \max(0, t) \equiv t\mathcal{H}(t)$  with  $\mathcal{H}$  the Heaviside function. For instance, taking a small parameter  $\eta > 0$ , we choose:

$$\phi_\eta(x) = \begin{cases} 0 & \text{for } x \in (-\infty; -\eta] \\ \frac{1}{4\eta}x^2 + \frac{1}{2}x + \frac{\eta}{4} & \text{for } x \in [-\eta; \eta] \\ x & \text{for } x \in [\eta; +\infty). \end{cases} \quad (3.2)$$

Note that the small parameter  $\eta$  is possibly different from  $\epsilon$  since  $\eta$  is a regularisation parameter for the non-smooth function  $\max(0, t)$ , while  $\epsilon$  is a penalisation parameter for the constraint to belong to  $K(\Omega)$ . We can then deduce a penalised variational formulation associated to (2.8):

$$\int_{\Omega} Ae(u) : e(v) dx + j'_{N,\epsilon}(u, v) = \int_{\Omega} f \cdot v dx + \int_{\Gamma_N} g \cdot v ds. \quad \forall v \in H_{\Gamma_0}^1(\Omega)^d, \quad (3.3)$$

where the directional derivative of (3.1) is

$$j'_{N,\epsilon}(u, v) = \frac{1}{\epsilon} \int_{\Gamma_c} \phi_\eta(u \cdot n) v \cdot n ds + \frac{1}{\epsilon} \int_S \phi_\eta([u] \cdot n_-) [v] \cdot n_- ds,$$

and an equivalent minimisation problem:

$$u = \operatorname{argmin}_{v \in H_{\Gamma_0}^1(\Omega)^d} \frac{1}{2} \int_{\Omega} Ae(v) : e(v) dx - \int_{\Omega} f \cdot v dx - \int_{\Gamma_N} g \cdot v ds + j_{N,\epsilon}(v).$$

Problems (2.12) and (2.14) cannot be written as minimisation problems, therefore we need to work directly on the variational inequality. The idea is to add a term  $j'_{N,\epsilon}(u, v - u)$  on the left hand side and change the spaces of the solutions as done in [16], chapter 3, keeping in mind that to get an equation we still need to regularise the friction term.

### 3.2. Regularisation of the friction term

In the friction models (2.10), (2.12), (2.14) and (2.16) we also need to regularise the norm  $\|\cdot\|$  to transform inequalities into equations. Let  $\mathcal{N}_\eta$  be a smooth function (at least twice differentiable) approximating the norm. For instance, following [16]:

$$\mathcal{N}_\eta(x) = \begin{cases} \|x\| & \text{for } \|x\| \geq \eta, \\ -\frac{1}{8\eta^3}\|x\|^4 + \frac{3}{4\eta}\|x\|^2 + \frac{3}{8}\eta & \text{for } \|x\| \leq \eta. \end{cases}$$

The new penalised and regularised equations are then given as follows.

- For the Tresca model:

$$\int_{\Omega} Ae(u) : e(v) dx + j'_{\text{tr},\eta}(u, v) + j'_{N,\epsilon}(u, v) = \int_{\Omega} f \cdot v dx + \int_{\Gamma_N} g \cdot v ds \quad \forall v \in H_{\Gamma_0}^1(\Omega)^d, \quad (3.4)$$

where  $j'_{\text{tr},\eta}(u, v)$  denotes the derivative of  $j_{\text{tr},\eta}$  at  $u$  in the direction  $v$  with

$$j_{\text{tr},\eta}(v) = \int_{\Gamma_c} \sigma_{\text{tr}} \mathcal{N}_\eta(v_t) ds + \int_S \sigma_{\text{tr}} \mathcal{N}_\eta([v]_t) ds.$$

The penalised and regularised Tresca problem can be written as a minimisation problem:

$$u = \operatorname{argmin}_{v \in H_{\Gamma_0}^1(\Omega)^d} \frac{1}{2} \int_{\Omega} Ae(v) : e(v) dx - \int_{\Omega} f \cdot v dx - \int_{\Gamma_N} g \cdot v ds + j_{N,\epsilon}(v) + j_{\text{tr},\eta}(v).$$

It is not the case for the other friction models described in the sequel.

- For the Coulomb model:

$$\int_{\Omega} Ae(u) : e(v) dx + j'_{\text{co},\epsilon,\eta}(u, v) + j'_{N,\epsilon}(u, v) = \int_{\Omega} f \cdot u dx + \int_{\Gamma_N} g \cdot u ds \quad \forall v \in H_{\Gamma_0}^1(\Omega)^d, \quad (3.5)$$

where

$$j'_{\text{co},\epsilon,\eta}(u, v) = \int_{\Gamma_c} \frac{\mu}{\epsilon} \phi_{\eta}(u \cdot n) \mathcal{N}'_{\eta}(u_t) \cdot v_t ds + \int_S \frac{\mu}{\epsilon} \phi_{\eta}([u] \cdot n_-) \mathcal{N}'_{\eta}([u]_t) \cdot [v]_t ds$$

and  $\mathcal{N}'_{\eta}$  is the derivative of  $\mathcal{N}_{\eta}$ .

- For the Norton-Hoff model:

$$\int_{\Omega} Ae(u) : e(v) dx + j_{\text{nh},\epsilon,\eta}(u, v) + j'_{N,\epsilon}(u, v) = \int_{\Omega} f \cdot v dx + \int_{\Gamma_N} g \cdot v ds \quad \forall v \in H_{\Gamma_0}^1(\Omega)^d, \quad (3.6)$$

where

$$j_{\text{nh},\epsilon,\eta}(u, v) = \int_{\Gamma_c} \frac{\mu}{\epsilon} \phi_{\eta}(u \cdot n) \mathcal{N}_{\eta}(u_t)^{\rho-1} u_t \cdot v_t ds + \int_S \frac{\mu}{\epsilon} \phi_{\eta}([u] \cdot n_-) \mathcal{N}_{\eta}([u]_t)^{\rho-1} [u]_t \cdot [v]_t ds.$$

- For the normal compliance model:

$$\int_{\Omega} Ae(u) : e(v) dx + j_{N,r,N_c}(u, v) + j'_{T,\eta,N_c}(u, v) = \int_{\Omega} f \cdot v dx + \int_{\Gamma_N} g \cdot v ds \quad \forall v \in H_{\Gamma_0}^1(\Omega)^d, \quad (3.7)$$

with

$$j_{N,\text{nc},r}(u, v) = \int_{\Gamma_c} C_N \phi_{\eta}(u \cdot n)^{m_N} v \cdot n ds + \int_S C_N \phi_{\eta}([u] \cdot n_-)^{m_N} [v] \cdot n ds,$$

$$j'_{T,\text{nc},\eta}(u, v) = \int_{\Gamma_c} C_T \phi_{\eta}(u \cdot n)^{m_T} \mathcal{N}'_{\eta}(u_t) \cdot v_t ds + \int_S C_T \phi_{\eta}([u] \cdot n_-)^{m_T} \mathcal{N}'_{\eta}([u]_t) \cdot [v]_t ds.$$

For this last model, both the normal and tangential terms were regularised but no penalisation is needed as the original equation is already posed in the whole space  $H_{\Gamma_0}^1(\Omega)^d$ .

We finally conclude that all regularised and penalised formulations (3.3), (3.4), (3.5), (3.6) and (3.7) can be written in full generality as non-linear variational formulation: find  $u \in H_{\Gamma_0}^1(\Omega)^d$  such that,

$$\int_{\Omega} Ae(u) : e(u) dx + \int_{S \cup \Gamma_c} j(u, v, n) ds = \int_{\Omega} f \cdot v dx + \int_{\Gamma_N} g \cdot v ds \quad \forall v \in H_{\Gamma_0}^1(\Omega)^d, \quad (3.8)$$

where the integrand  $j(u, v, n)$  is non-linear with respect to the solution  $u$  but linear with respect to the test function  $v$ .

### 3.3. Differentiability of the penalised and regularised terms

The fact that  $\phi_{\eta}$ , defined by (3.2), is smooth does not imply it is Fréchet differentiable from  $L^2(\Gamma_c)$  to  $L^2(\Gamma_c)$ , see section 4.3 in [63]. It only implies the Gâteaux differentiability at each point  $x \in \Gamma_c$ . Nevertheless we can state the following lemma.

**Lemma 3.1.** *The functional  $u \rightarrow \phi_{\eta}(u)$  is differentiable from  $H^{\frac{1}{2}}(\Gamma_c)$  into  $L^2(\Gamma_c)$ , and from  $H^{\frac{1}{2}}(S)$  into  $L^2(S)$ .*

**Proof.** This is an application of theorem 7 in [19]. We introduce the Nemytskij operator (associated with  $\phi_{\eta}$ )  $\Phi_{\eta} : u \rightarrow \phi_{\eta}(u)$  where  $u \in L^p(\Gamma_c) \cap L^p(S)$  with  $p$  fixed later on. This theorem ensures its Fréchet differentiability from  $L^p(\Gamma_c) \cap L^p(S)$  to  $L^2(\Gamma_c) \cap L^2(S)$  if the following conditions are fulfilled:

- $\phi_{\eta}$  is a  $C^1$  function from  $\mathbb{R}$  to  $\mathbb{R}$ .

- The Nemytskij operator associated with  $\phi'_\eta$  is continuous from  $L^p(\Gamma_c) \cap L^p(S)$  to  $L^r(\Gamma_c) \cap L^r(S)$  with  $r = 2p/(p-2)$ .

As  $u \in H^{\frac{1}{2}}(\Gamma_c) \cap H^{\frac{1}{2}}(S)$ , by Sobolev embeddings we deduce  $u \in L^p(\Gamma_c) \cap L^p(S)$  with  $p = 2(d-1)/(d-3/2)$ . This means that  $r = 4(d-1)$ . It is clear that  $y \rightarrow \phi'_\eta(y)$  exists and is continuous ( $\phi'_\eta$  is also globally Lipschitz continuous). Due to the choice of the penalisation,  $\phi'_\eta$  is bounded (depending on the parameter of penalisation). Remark 4 in [19] then implies the continuity from  $L^p(\Gamma_c) \cap L^p(S)$  to  $L^r(\Gamma_c) \cap L^r(S)$  with  $r = 2p/(p-2)$ . ■

**Remark 3.2.** As  $u \in H^1_{\Gamma_0}(\Omega)^d$ , it follows that  $u \cdot n \in H^{\frac{1}{2}}(\Gamma_c) \cap H^{\frac{1}{2}}(S)$  for  $\Omega$  smooth enough. Then  $u \rightarrow \phi_\eta(u \cdot n)$  is Fréchet differentiable from  $H^1_{\Gamma_0}(\Omega)^d$  into  $L^2(\Gamma_c) \cap L^2(S)$ .

**Remark 3.3.** The regularisation term  $\mathcal{N}_\eta$  is twice differentiable from  $\mathbb{R}^d$  to  $\mathbb{R}^d$ . Moreover its derivative is bounded, so, thanks to theorem 8 in [19], it is Gâteaux differentiable from  $L^2(\Gamma_c) \cap L^2(S)$  into  $L^2(\Gamma_c) \cap L^2(S)$ . As its second derivative is bounded by a linear function, it is also twice Fréchet differentiable from  $H^{\frac{1}{2}}(\Gamma_c) \cap H^{\frac{1}{2}}(S)$  into  $L^2(\Gamma_c) \cap L^2(S)$ , thanks to theorem 7 in [19] applied two times. The proof is the same as in Lemma 3.1.

### 3.4. Existence and uniqueness of the penalised/regularised formulation

For (3.3) and (3.4), existence and uniqueness results are easily proved by taking advantage of their respective minimisation problem formulations.

**Theorem 3.4.** *The problems (3.4) and (3.3) admit a unique solution  $u \in H^1_{\Gamma_0}(\Omega)^d$ , when  $f \in L^2(\Omega)^d$ ,  $g \in L^2(\Gamma_N)^d$ ,  $\phi_\eta$  is positive increasing and  $\mathcal{N}_\eta$  is convex positive.*

**Proof.** We introduce the functional:

$$E(u) = \frac{1}{2}a(u, u) + \frac{1}{\epsilon} \left( \int_{\Gamma_c} \int_0^{u \cdot n} \phi_\eta(t) dt ds + \int_S \int_0^{[u] \cdot n} \phi_\eta(t) dt ds \right) + j_\eta(u) - \int_{\Gamma_N} g \cdot u ds - \int_\Omega f \cdot u dx$$

with  $a(u, u) = \int_\Omega Ae(u) : e(u) dx$  and  $j_\eta(u) = 0$  for (3.3) and  $j_\eta(u) = \int_{\Gamma_c} \sigma_{\text{tr}} \mathcal{N}_\eta(u_t) ds + \int_S \sigma_{\text{tr}} \mathcal{N}_\eta([u]_t) ds$  for (3.4). Thanks to Korn inequality,  $u \rightarrow a(u, u)$  is strictly convex. We now prove that  $\psi : u \rightarrow \int_{\Gamma_c} \frac{1}{\epsilon} \int_0^{u \cdot n} \phi_\eta(t) dt ds$  is convex. We compute the Hessian of  $\psi$ :

$$D^2\psi(u)(h, h') = \int_{\Gamma_c} \frac{1}{\epsilon} \phi'_\eta(u \cdot n) h' \cdot n h \cdot n ds$$

which is positive as  $\phi'_\eta$  is positive. Moreover, since  $\mathcal{N}_\eta$  is convex,  $j_\eta$  is convex and lower semi-continuous. So  $u \rightarrow E(u)$  is strictly convex and lower semi-continuous on  $H^1_{\Gamma_0}(\Omega)^d$ . It is also bounded below as  $\phi_\eta$  is non-negative and an approximation of  $x \rightarrow x\mathcal{H}(x)$  (for instance  $\phi_\eta([u] \cdot n)$  vanishes when  $[u] \cdot n$  is smaller than  $-\eta$ ). It ensures the existence of a unique minimiser of  $E$  on  $H^1_{\Gamma_0}(\Omega)^d$ . To conclude we just need to remark that the optimality criterion is exactly (3.3) or (3.4), therefore both admit one and only one solution. ■

We now turn to the other models. For (3.5) the existence is proved in chapter 3 of [16]. A proof similar to that for (3.5) can be done for (3.6). For these two cases, the uniqueness is not ensured. For the normal compliance model we refer to [20] for existence and uniqueness.

#### 4. Optimisation problem

Our goal is to minimise a certain function  $J(\Omega)$  depending on  $u$ , the displacement which solves one of the contact formulations given in Section 2, under constraints also depending on  $u$ , denoted by  $I(\Omega)$ :

$$\begin{cases} \min J(\Omega) \\ \Omega \in \mathcal{U}_{ad} \\ u \text{ solution of (3.8)} \\ I(\Omega) \leq 0 \end{cases} \quad (4.1)$$

where  $\mathcal{U}_{ad}$  is the set of admissible shapes. Typically, admissible shapes  $\Omega$  should be included into a fixed domain  $D$  and the Dirichlet boundary  $\Gamma_0 \subset \partial D$  is not allowed to change. In the following we denote  $\Gamma_m$  the part of the boundary of  $\Omega$  which is allowed to change.

##### 4.1. Shape derivative

To minimise (4.1) we apply a gradient method, therefore we need to compute derivatives with respect to  $\Omega$ . We choose to use the notion introduced by Hadamard and then extensively studied, see for instance [28], [46], [53], [57] or [58]. Starting from a smooth domain  $\Omega_0$ , the variation of the domain takes the form:

$$\Omega_\theta = (Id + \theta)(\Omega_0)$$

with  $\theta \in W^{1,\infty}(\mathbb{R}^d, \mathbb{R}^d)$  and  $Id$  the identity map. When  $\theta$  is sufficiently small,  $Id + \theta$  is a diffeomorphism in  $\mathbb{R}^d$ , see [1]. Once the variation of the shape is defined, it is possible to define the notion of Gâteaux derivative for a function  $J$  depending on the shape.

**Definition 4.1.** The shape derivative  $J'(\Omega)(\theta)$  of  $J(\Omega)$  at  $\Omega$  in the direction  $\theta$  is defined as the derivative at 0 of the application  $t \rightarrow J((Id + t\theta)(\Omega))$  which means:

$$J((Id + t\theta)(\Omega)) = J(\Omega) + tJ'(\Omega)(\theta) + o(t)$$

where  $J'(\Omega)$  is a continuous linear form on  $W^{1,\infty}(\mathbb{R}^d, \mathbb{R}^d)$ .

We recall the following classical theorem [1] which will be used in the next section.

**Theorem 4.2.** Let  $\Omega \in \mathcal{U}_{ad}$  be a smooth open domain,  $\phi$  a smooth function defined in  $\mathbb{R}^d$ ,

$$J_v(\Omega) = \int_{\Omega} \phi(x) dx \quad \text{and} \quad J_s(\Omega) = \int_{\partial\Omega} \phi(x) ds.$$

These two functions are shape differentiable at  $\Omega$  in the direction  $\theta \in W^{1,\infty}(\mathbb{R}, \mathbb{R})$  and

$$J'_v(\Omega)(\theta) = \int_{\partial\Omega} \theta \cdot n \phi ds \quad \text{and} \quad J'_s(\Omega)(\theta) = \int_{\partial\Omega} \theta \cdot n \left( \frac{\partial\phi}{\partial n} + H\phi \right) ds$$

where  $H = \text{div}(n)$  is the mean curvature of  $\partial\Omega$ .

We also give the shape derivative of the normal (see proposition 5.4.14 in [28]).

**Proposition 4.3.** Let  $\Omega$  be a  $C^2$  domain and  $n \in C^1(\mathbb{R}^d, \mathbb{R}^d)$  an extension of the unit normal to  $\partial\Omega$ . Denote  $\Omega_{t\theta} = \Phi(t)\Omega_0$  with  $\Phi(t) = (Id + t\theta)$ . Then:

$$t \rightarrow n_t = \frac{w(t)}{\|w(t)\|} \quad \text{with} \quad w(t) = (\nabla^T \Phi(t)^{-1} n) \circ \Phi(t)^{-1}$$

is an extension to the normal of  $\partial\Omega_{t\theta}$ , is differentiable in 0 and its derivative is:

$$n'(\theta) = -\nabla_t(\theta \cdot n) \quad \text{on} \quad \partial\Omega$$

where  $\nabla_t \zeta = \nabla \zeta - (\nabla \zeta \cdot n)n$  is the tangential gradient of a function  $\zeta$ .

4.1.1. *General case*

We proceed to the computation of the gradient of a general criterion:

$$J(\Omega) = \int_{\Omega} m(u) dx + \int_{\Gamma_m} l(u) ds \quad (4.2)$$

where  $\Gamma_m$  is the part of  $\partial\Omega$  allowed to move during the optimisation process,  $m$  and  $l$  are smooth functions from  $\mathbb{R}^d$  into  $\mathbb{R}$ , verifying

$$\begin{aligned} |m(u)| &\leq C(1 + |u|^2) \\ |m'(u) \cdot h| &\leq C'|u||h| \end{aligned}$$

and

$$\begin{aligned} |l(u)| &\leq C(1 + |u|^2) \\ |l'(u) \cdot h| &\leq C'|u||h| \end{aligned}$$

for every  $u, h \in \mathbb{R}^d$  with  $C > 0$  and  $C' > 0$ . Note that (4.2) is thus well defined for  $u \in H^1(\Omega)^d$ .

In the next theorem, we shall consider the solution  $u$  of the non-linear variational equation (3.8) which involves the function  $j(u, p, n)$  (the precise form of which differs according to the considered penalised and regularised contact model). In order to distinguish the normal derivative  $\partial j / \partial n$  from the partial derivative of  $j(u, p, n)$  with respect to its third argument, we now consider  $j$  as a function of three arguments  $(u, p, \lambda) \in \mathbb{R}^d \times \mathbb{R}^d \times \mathbb{R}^d \rightarrow \mathbb{R}$  and the derivative with respect to  $n$  of  $j(u, p, n)$  is denoted:

$$\frac{\partial j}{\partial \lambda}(u, p, n).$$

**Theorem 4.4.** *Assume that  $\Gamma_m \cap \Gamma_0 = \emptyset$ ,  $f \in H^1(\mathbb{R}^d)^d$  and  $g \in H^2(\mathbb{R}^d)^d$ . Assume that (3.8) admits a unique solution  $u \in H_{\Gamma_0}^1(\Omega)^d$ , not only for  $\Omega$  but also for all its admissible variations  $(Id + t\theta)(\Omega)$  for  $t$  small enough and  $\theta \in W^{1,\infty}(\mathbb{R}^d, \mathbb{R}^d)$ . If we denote  $J'(\Omega)(\theta)$  the Gâteaux derivative of  $J(\Omega)$  with respect to  $\Omega$  in the direction  $\theta \in W^{1,\infty}(\mathbb{R}^d, \mathbb{R}^d)$ , we have:*

$$\begin{aligned} J'(\Omega)(\theta) &= \int_{\Gamma_m} (\theta \cdot n)(m(u) + Ae(u) : e(p) - f \cdot p) ds \\ &\quad + \int_{\Gamma_m} (\theta \cdot n) \left( Hl(u) + \frac{\partial l(u)}{\partial n} \right) \\ &\quad - \int_{\Gamma_N \cap \Gamma_m} (\theta \cdot n) \left( Hp \cdot g + \frac{\partial(p \cdot g)}{\partial n} \right) ds \\ &\quad + \int_{S \cup \Gamma_c} (\theta \cdot n) \left( Hj(u, p, n) + \frac{\partial j(u, p, n)}{\partial n} \right) ds \\ &\quad + \int_{S \cup \Gamma_c} \frac{\partial j}{\partial \lambda}(u, p, n) \cdot n'(\theta) ds \end{aligned} \quad (4.3)$$

where  $n'(\theta)$  is the shape derivative of the normal (on  $S$  it is the shape derivative of  $n_-$ ) and  $p$  is defined as the solution of the following adjoint problem:

$$\begin{aligned} \int_{\Omega} Ae(p) : e(\psi) dx + \int_{\Omega} m'(u) \cdot \psi dx + \int_{\Gamma_m} l'(u) \cdot \psi ds \\ + \int_{S \cup \Gamma_c} \frac{\partial j}{\partial u}(u, p, n) \cdot \psi ds = 0 \quad \forall \psi \in H_{\Gamma_0}^1(\Omega)^d. \end{aligned} \quad (4.4)$$

**Proof.** The proof relies on C ea's method [10] or [1]. A rigorous proof would require to prove that  $u$  is Gâteaux differentiable with respect to the shape. This could be done by making in the non-linear regularised formulation (3.8) a change of variable to transport integrals on the reference domain  $\Omega_0$

such that  $\Omega = (Id + t\theta)(\Omega_0)$ . This leads to an equation of the type:  $F(u, t) = 0$  with  $F$  differentiable with respect to  $t$ , thanks to Remark 3.3 and Lemma 3.1. Applying the implicit function theorem at  $t = 0$  yields the desired result. Assuming this point proved, we give a (formal) proof of the theorem by means of the Lagrangian method, noting  $u'(\theta)$  the shape derivative of  $u$ . Let us introduce the Lagrangian  $L$  with  $v$  and  $q$  in  $H_{\Gamma_0}^1(\mathbb{R}^d)^d$ :

$$\begin{aligned} L(v, q, n(\Omega), \Omega) &= \int_{\Omega} m(v) dx + \int_{\Gamma_m} l(v) ds + \int_{\Omega} Ae(v) : e(q) dx \\ &+ \int_{S \cup \Gamma_c} j(v, q, n) ds - \int_{\Omega} f \cdot q dx - \int_{\Gamma_N} g \cdot q ds. \end{aligned}$$

Recall that  $j(v, q, n)$ , defined in (3.8), is a linear function of  $q$ . Thus, the Lagrangian  $L$  is linear with respect to the adjoint variable  $q$  too, as it should be. Since  $\Gamma_0$  is fixed, there is no need of a Lagrange multiplier for the Dirichlet condition in the Lagrangian:  $\Gamma_0 \subset \partial\Omega$  for every  $\Omega \in \mathcal{U}_{ad}$ . Moreover the functions  $q$  and  $v$  are in spaces independent of  $\Omega \in \mathcal{U}_{ad}$ . We note  $(u, p)$  a stationarity point of  $L$ . The state equation (3.8) can be retrieved by differentiating  $L$  with respect to  $q$  in the direction  $\psi \in H_{\Gamma_0}^1(\mathbb{R}^d)^d$ :

$$\left\langle \frac{\partial L}{\partial q}(u, q, n, \Omega), \psi \right\rangle = 0 \quad \forall \psi \in H_{\Gamma_0}^1(\mathbb{R}^d)^d.$$

Similarly, the adjoint equation (4.4), solved by  $p$ , is found by differentiating  $L$  with respect to  $v$  in the direction  $\psi \in H_{\Gamma_0}^1(\mathbb{R}^d)^d$ :

$$\left\langle \frac{\partial L}{\partial v}(u, p, n, \Omega), \psi \right\rangle = \int_{\Omega} Ae(v) : e(\psi) dx + \int_{\Omega} m'(u) \cdot \psi dx + \int_{\Gamma_m} l'(u) \cdot \psi ds + \int_{S \cup \Gamma_c} \frac{\partial j}{\partial u}(u, p, n) \cdot \psi ds$$

and the adjoint variational formulation is deduced by making the above term zero.

To find the shape derivative of  $J(\Omega)$ , we remark that:

$$J(\Omega) = L(u(\Omega), q, n(\Omega), \Omega)$$

and differentiate  $L$  with respect to the shape in the direction  $\theta$  which gives:

$$\begin{aligned} J'(\Omega, \theta) &= L'(\Omega, u_{\Omega}, q, n_{\Omega}; \theta) \\ &= \partial_{\Omega} L(\Omega, u_{\Omega}, q, n_{\Omega}; \theta) + \left\langle \frac{\partial L}{\partial v}(\Omega, u_{\Omega}, q, n_{\Omega}), u'(\theta) \right\rangle + \left\langle \frac{\partial L}{\partial \lambda}(\Omega, u_{\Omega}, q, n_{\Omega}), n'(\theta) \right\rangle. \end{aligned}$$

But, as  $u'(\theta) \in H_{\Gamma_0}^1(\Omega)^d$ , taking  $q = p(\Omega)$  leads to:

$$\left\langle \frac{\partial L}{\partial v}(\Omega, u_{\Omega}, p(\Omega), n_{\Omega}), u'(\theta) \right\rangle = 0.$$

Consequently:

$$J'(\Omega, \theta) = L'(\Omega, u_{\Omega}, p_{\Omega}, n_{\Omega}; \theta) = \partial_{\Omega} L(\Omega, u_{\Omega}, p_{\Omega}, n_{\Omega}; \theta) + \left\langle \frac{\partial L}{\partial \lambda}(\Omega, u_{\Omega}, p_{\Omega}, n_{\Omega}), n'(\theta) \right\rangle.$$

By using the formulae of Theorem 4.2, we recover (4.3). ■

**Remark 4.5.** The derivative found in Theorem 4.4 is correct only if the solution  $u$  exists and is unique for all admissible domains. Nevertheless, in numerical practice we will use Theorem 4.4 even for models where no uniqueness results are known.

## 4.2. Criteria

### 4.2.1. Compliance and volume

In some numerical examples we will use these two classical criteria which can be written under the form of (4.2). For the compliance:

$$m_{Comp}(u) = f \cdot u$$

$$l_{Comp}(u) = g \cdot u.$$

For the volume:

$$m_{vol}(u) = 1$$

$$l_{vol}(u) = 0.$$

#### 4.2.2. Normal force

The normal force, which is always non-positive (see (2.6)), is the force which is applied on the structure at the contact surface. It takes the following form:  $Ae(u)n \cdot n$  on  $\Gamma_c$  and  $Ae(u|_{S_-})n_- \cdot n_-$  on  $S$ . In the penalised and regularised formulations the normal force  $P_N$  is now given by a different formula:

$$P_N = \begin{cases} -\frac{1}{\epsilon}\phi_\eta(u \cdot n) & \text{on } \Gamma_c \\ -\frac{1}{\epsilon}\phi_\eta([u] \cdot n_-) & \text{on } S \end{cases} \quad (4.5)$$

where  $\phi_\eta(x)$  was defined in (3.2) as a smooth approximation of  $\max(0, x)$  and  $\epsilon$  is the penalisation parameter defined in (3.1).

The various criteria we consider, depending on the normal force, are of the form:

$$l(u) = l_i(P_N(u), c)\mathbf{1}_{S \cup \Gamma_c}$$

where  $\mathbf{1}_{S \cup \Gamma_c}$  is the characteristic function of  $S \cup \Gamma_c$ ,  $c$  is a constant and  $l_i$  is defined according to how we want to control the normal force.

**Uniformisation:** If we want to make the normal force  $P_N$  uniform around a constant  $c < 0$  on the contact zone, we introduce the following function:

$$l_1(P_N, c) = (P_N - c)^2. \quad (4.6)$$

**Minimising the maximum of the normal force:** If we want to force the normal force  $P_N$  to be under a certain threshold  $c < 0$ , we define:

$$l_2(P_N, c) = \max(P_N - c, 0)^2.$$

However, this could lead to a null gradient during the optimisation process due, for example, to a null adjoint  $p$  when there is no point in contact. This could be a big hurdle when the initial shape in the optimisation process is such that there is no contact. Indeed the gradient does not indicate that contact is possible and how to reach a shape where there is an effective contact. So we change the definition (4.5) of  $P_N$  by introducing the following function:

$$\phi_\eta^{th}(x) = \begin{cases} \phi_\eta(x) - \phi_\eta(0) & \text{if } x \geq 0 \\ \phi'_\eta(0)x & \text{otherwise.} \end{cases}$$

We plot the corresponding functions  $\phi_\eta$  and  $\phi_\eta^{th}$  on Figure 4.1. Then we define:

$$P_N^{th} = \begin{cases} -\frac{1}{\epsilon}\phi_\eta^{th}(u \cdot n) & \text{on } \Gamma_c \\ -\frac{1}{\epsilon}\phi_\eta^{th}([u] \cdot n_-) & \text{on } S. \end{cases}$$

Now when  $u \cdot n = 0$ , the normal force is set to 0 and when  $u \cdot n < 0$ , the force is non-negative and

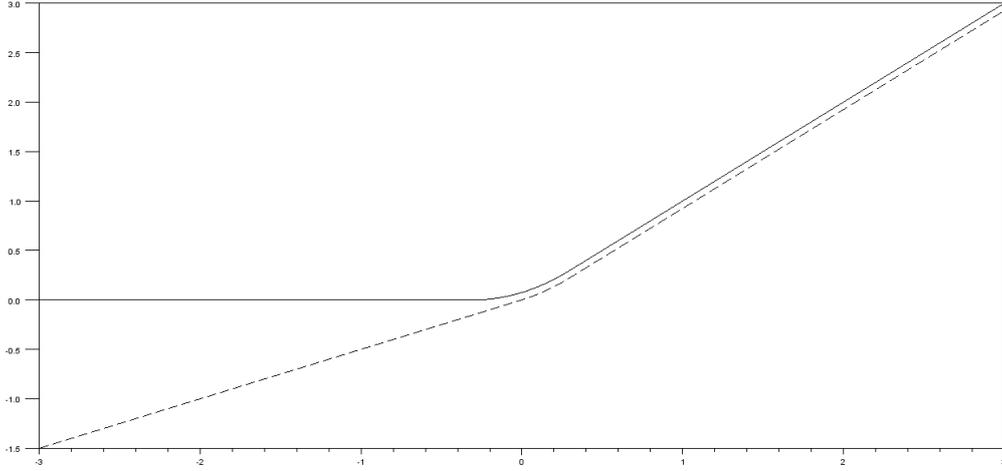


FIGURE 4.1. The functions  $\phi_\eta$  (continuous curve) and  $\phi_\eta^{th}$  (dashed curve).

decreases linearly, giving a sense to an opposite normal force when there is no contact. Making the most of this new normal force formulation, we define the following criterion:

$$l_3(P_N^{th}, c) = \begin{cases} 1 - \frac{P_N^{th}}{c} & \text{if } P_N^{th} \leq 0 \\ e^{-\frac{P_N^{th}}{c}} & \text{if } P_N^{th} > 0. \end{cases} \quad (4.7)$$

The bigger  $\frac{P_N^{th}}{c}$ , the smaller is  $l_3(P_N^{th}, c)$ . Other formulas for  $l_3$  are also possible and give similar results to those obtained with (4.7).

## 5. Numerical implementation

### 5.1. The level set method

As we choose to define the shape thanks to a level set, we recall the framework of this method introduced by Osher and Sethian in [49], [48] and [56]. Let  $D \subset \mathbb{R}^d$  be a bounded domain in which all admissible shapes  $\Omega$  are included. The boundary of  $\Omega$  is located thanks to the level set function  $\psi$ , defined in  $D$  by

$$\begin{cases} \psi(x) = 0 & \text{if } x \in \partial\Omega \cap D \\ \psi(x) < 0 & \text{if } x \in \Omega \\ \psi(x) > 0 & \text{otherwise.} \end{cases}$$

The normal  $n$  and the mean curvature  $H$  of the shape  $\Omega$  are respectively given by  $\frac{\nabla\psi}{\|\psi\|}$  and  $\text{div}\left(\frac{\nabla\psi}{\|\psi\|}\right)$ . These quantities are computed throughout the whole domain  $D$  which naturally defines extensions of their first definition on  $\partial\Omega$ .

### 5.2. Optimisation algorithm

The optimisation process produces a sequence  $(\Omega_i)_{i \in \mathbb{N}}$  of shapes. We start with an initial shape  $\Omega_0$  and compute iteratively the sequence. To make the level set evolve from  $\Omega_i$  to  $\Omega_{i+1}$ , the Hamilton

Jacobi transport equation [49] is solved for  $t \in [0, t_f]$ :

$$\frac{\partial \psi}{\partial t} + V \|\nabla \psi\| = 0 \text{ in } D \quad (5.1)$$

where  $V(x)$  is the normal velocity of the shape's boundary. The equation (5.1) is obtained by differentiating:  $\psi(t, x(t)) = \text{const}$  and replacing  $\dot{x}(t)$  by  $Vn$ . Thanks to  $\psi(x, t)$  we can define  $\Omega_i(t)$  for every  $t \in [0, t_f]$  and choose  $\Omega_{i+1} = \Omega_i(t_f)$  for an appropriate  $t_f$  which corresponds to the descent step. The speed  $V$ , defined everywhere in  $D$  to be able to solve (5.1), is chosen, through a SLP (Successive Linear Programming, or Sequential Linear Programming) type algorithm, thanks to the criteria's gradients calculated on  $\Omega_i$  using theorem 4.4 and plays the role of a descent direction. The time step size  $t_f$  is at first chosen equal to an arbitrary  $t_{\max}$  and then decreases until an admissible shape is found (if not the algorithm stops). When an admissible shape is reached, the time step  $t_f$  is allowed to grow. We distinguish two phases in the algorithm: first, if the current shape does not fulfil the constraints: we authorise the objective to slowly increase as long as the constraints improve. Then, once an admissible shape is reached, we reject every future shape which, either makes the objective increase or is not admissible.

The Hamilton Jacobi equation (5.1) is solved by an explicit second order upwind scheme on a cartesian grid meshing  $D$  with Neumann boundary conditions. Since the scheme is explicit in time, the time stepping has to satisfy a CFL condition and, in order to regularise the level set which can become too flat or too steep during the successive optimisation iterations, periodic reinitialisations, thanks to an Hamilton Jacobi equation admitting the signed distance to the shape as stationary solution, are performed. We refer to [2] for numerical implementation details.

### 5.3. Finite element method

Using the same cartesian grid, we choose to solve the contact and adjoint equations on the whole domain  $D$  using the "ersatz material" approach, thanks to the quadrangular finite elements. It is tantamount to fill  $D \setminus \Omega$  with a weak material mimicking void but preventing the stiffness matrix from being singular. This technique is commonly used in topology optimisation with level sets [2], [64].

Concerning the non-linear penalised equations, they are usually solved by a damped Newton method, see [12] chapter 6, or a fixed point method. The Newton method has the advantage to be faster but it needs a good choice for the damping. On the other hand, the fixed point method, despite its relative slowness, is easier to implement. The robustness of the algorithm which solves the contact equations is crucial in the optimisation process. First because the optimisation can produce structures for which the finite element matrices are nearly singular. Secondly because we are solving problems whose solution is not always unique. This leads to difficulties which can be seen in Examples 11 and 12 below. The contact problems are solved (thanks to the finite element method) by discretising the contact region and applying node to node contact conditions for the auto-contact part. We choose to use a fixed point method for the computation of the non-linear problems solutions considered, which converges in, at most, 300 iterations with an average of 100.

## 6. Numerical examples

This section is divided into three subsections. The first one is a study of the sensitivity of the shape optimisation with respect to the penalisation parameter in the case of frictionless contact. The two next ones correspond respectively to 2D and 3D examples in which the parameters are fixed. In all the examples of this section, the contact zone is fixed (non-optimisable) but the structure can choose to use it or not. In each subsection, different models are used depending on the mechanical case. In 2D, the computational domain  $D$  is always a square of size  $2 \times 2$ . Except for Examples 5, 11 and

Pena. param. $\epsilon$	Volume	Compliance	Compliance Constraint	Iterations	Evaluations
$\epsilon = 10^{-2}$	1.86605	19.9999	20	33	49
$\epsilon = 10^{-3}$	1.86508	19.9975	20	39	54
$\epsilon = 10^{-4}$	1.86421	19.9991	20	32	47
$\epsilon = 10^{-5}$	1.86412	19.9997	20	31	46
$\epsilon = 10^{-6}$	1.86405	19.9998	20	29	44
$\epsilon = 10^{-7}$	1.86357	19.9956	20	36	51
$\epsilon = 10^{-8}$	1.86357	19.9956	20	36	51
$\epsilon = 10^{-9}$	1.86358	19.9955	20	36	51
$\epsilon = 10^{-10}$	1.86349	19.9964	20	36	51

TABLE 6.1. Results for different penalisation parameters for example 0.

12, where  $D$  is discretised with 2500 square elements, for all other examples,  $D$  is discretised with 6400 square elements. For the 3D examples, only the sliding contact model and Tresca friction contact model are tested. Except in Example 14 where  $D$  is a cylinder of radius 1 and height 1, the domain  $D$  is a rectangular parallelepiped of dimension  $1 \times 2 \times 1$  meshed with tetrahedra. In all 2D examples, except Example 3, there is no volume force and only unit point surface forces are applied. In 2D the Young modulus is set to  $E = 1$  and the Poisson coefficient is  $\nu = 0.3$ . In 3D, we take  $E = 210000$  and  $\nu = 0.3$ . In 2D and 3D, the penalisation coefficient  $\epsilon$  is set to  $10^{-7}$ . During the optimisation process, some shapes are rejected either because they do not fulfil the constraints or because they do not decrease the objective function. Due to this fact, for each example, both the number of iterations (shapes which were accepted) and the number of evaluations (all the shapes which were evaluated) are given.

### 6.1. Study of the sensitivity to the penalisation

For two examples, we vary the penalisation parameter  $\epsilon$  in (3.1) from  $10^{-2}$  to  $10^{-10}$  and look at the sensitivity of the shape optimisation problem with respect to this parameter  $\epsilon$ . For each example we minimise the volume under a compliance constraint. The potential contact zone is drawn in green, the arrows represent the forces and black zones the part of the boundary where Dirichlet conditions are prescribed, in all the directions (otherwise mentioned).

- Example 0, a unit force ( $\Gamma_N$ ) is applied at the point  $(2, 1)$ , the left side of the structure ( $\Gamma_0$ ) is fixed and  $\Gamma_c = \emptyset$ . We show the different final designs found in Figure 6.1. The Results are shown in Table 6.1.

This example is interesting as it provides both a contact zone which opens and a contact zone which is in actual contact. There is almost no (or very tiny) dependence on the penalisation parameter, as far as final designs, final values of objective and constraints and numbers of iterations and evaluations are concerned. This shows that the shape optimisation problem is almost insensitive to the value of the penalisation.

- Example 1, Dirichlet conditions ( $\Gamma_0$ ) are enforced on the whole left side,  $\Gamma_c = \emptyset$  and a downward unit force ( $\Gamma_N$ ) is applied at the point  $(2, 1.5)$ . This example is almost trivial for our sensitivity study since it turns out that the only possible contact zone is never in contact and, so, the penalisation parameter should not play any role. Therefore, as can be expected for this example, the penalisation parameter has indeed no impact on the shape optimisation. The final designs are the same (one is shown in Figure 6.2 next to the load case representation). The number of

SHAPE OPTIMISATION FOR CONTACT PROBLEMS

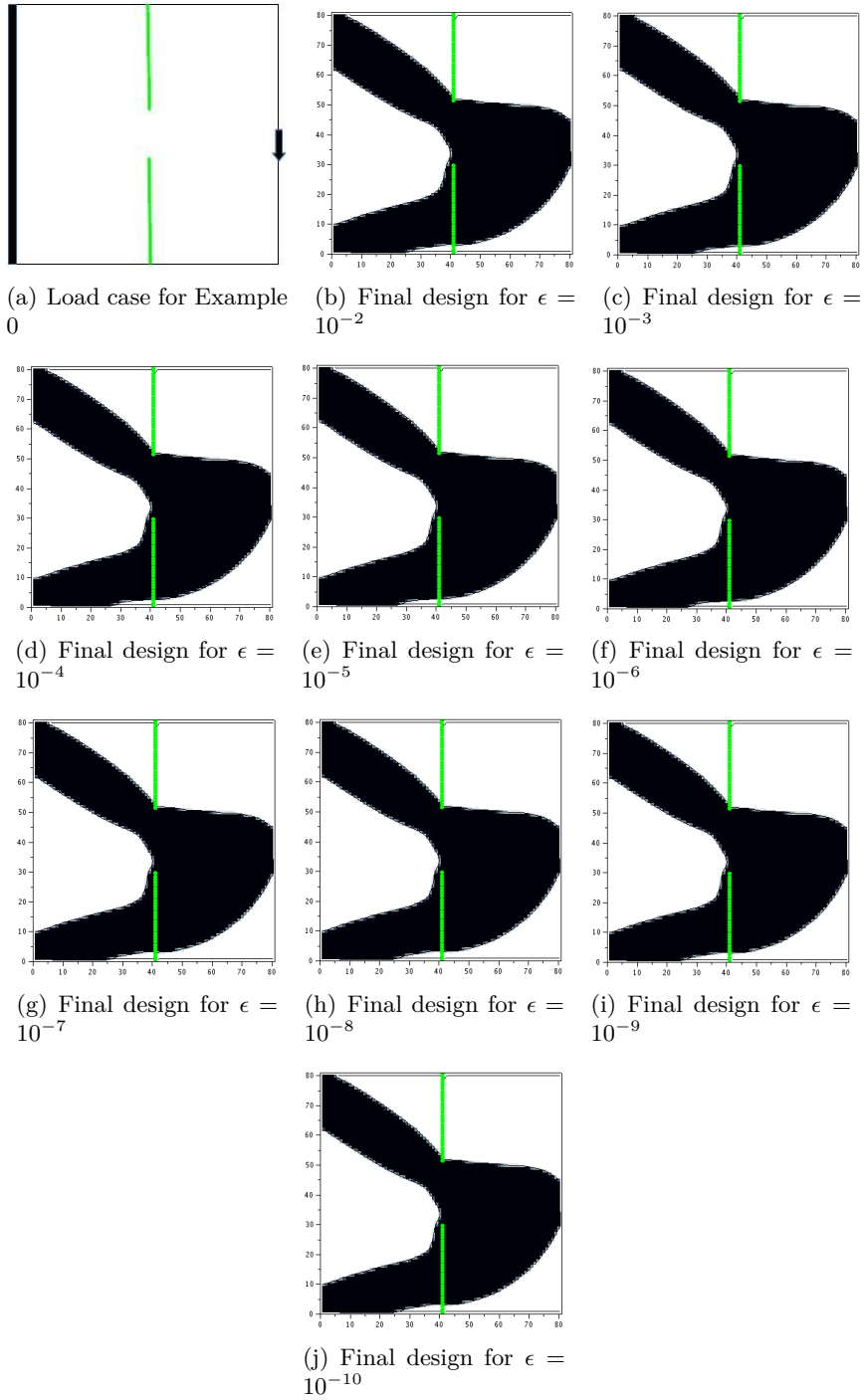


FIGURE 6.1. Example 0

iterations is always 30 and the number of evaluations 46. The final volume value is 1.6375 and the compliance constraint is 19.9999 for a possible maximum of 20.

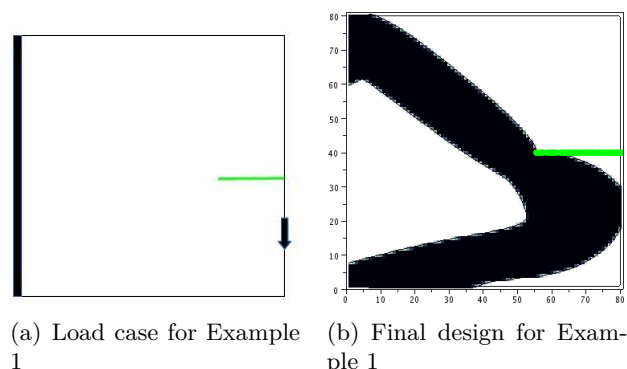


FIGURE 6.2. Example 1

## 6.2. Examples in 2D

### 6.2.1. Sliding contact

We present five examples (labeled from 2 to 5) where the volume is minimised under a compliance constraint (the value of this constraint is given in Table 6.2). The potential contact zone is drawn in green, the arrows represent the forces and black zones the part of the boundary where Dirichlet conditions are prescribed, in all the directions (otherwise mentioned). The results are collected in Table 6.2.

- Example 2, Dirichlet conditions ( $\Gamma_0$ ) are enforced on the whole left side,  $\Gamma_c = \emptyset$  and a unit downward force ( $\Gamma_N$ ) is applied at the point  $(2, 1.5)$ . Example 1-2bis is the same example as 1 and 2 without the contact zone. Results are presented in Figures 6.3 and 6.4.

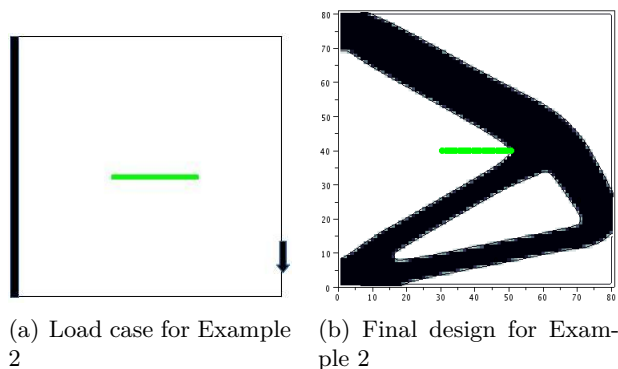


FIGURE 6.3. Example 2

- Example 3, Dirichlet conditions ( $\Gamma_0$ ) are enforced on the whole left side,  $\Gamma_c = \emptyset$  and a rightward force ( $\Gamma_N$ ) is applied on the segment from  $(2, 0.8)$  to  $(2, 1.2)$ . Example 3bis is similar without the contact area. Results are given in Figures 6.5 and 6.6.
- Example 4, Dirichlet conditions ( $\Gamma_0$ ) are enforced on the whole left side,  $\Gamma_c = \emptyset$  and a unit upward force ( $\Gamma_N$ ) is applied at  $(2, 1.5)$ . Example 4bis is similar without the contact boundary conditions. Results can be seen in Figures 6.7 and 6.8.

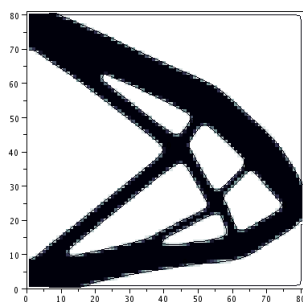
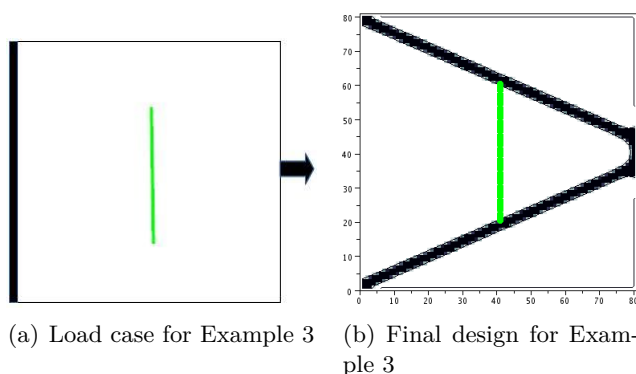


FIGURE 6.4. Final design for Example 1-2bis



(a) Load case for Example 3

(b) Final design for Example 3

FIGURE 6.5. Example 3

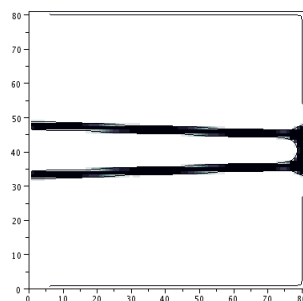


FIGURE 6.6. Final design for Example 3bis

- Example 5, Dirichlet conditions ( $\Gamma_0$ ) are enforced on the top boundary of the L-shape,  $S = \emptyset$  and a unit downward force ( $\Gamma_N$ ) is applied at  $(2, 1.6)$ . Example 5bis corresponds to the same problem without the contact part. Results are shown in Figures 6.9 and 6.10.

In Examples 1, 2, and 3, the optimisation algorithm tends to avoid the contact zone which is not the case when this zone is removed. Indeed, due to the direction of the forces, this zone opens and no point is in contact. Including it in the structure would increase the compliance, which is not possible by virtue of the constraint on the compliance. In Example 4, the points of the contact zone are in contact and including them in the structure does not imply a too big increase of the compliance, despite the sliding occurrence. In Example 5, the contribution of the contact boundary conditions is underlined by the fact that, for the same optimisation problem without contact (Example 5bis), even the full-domain

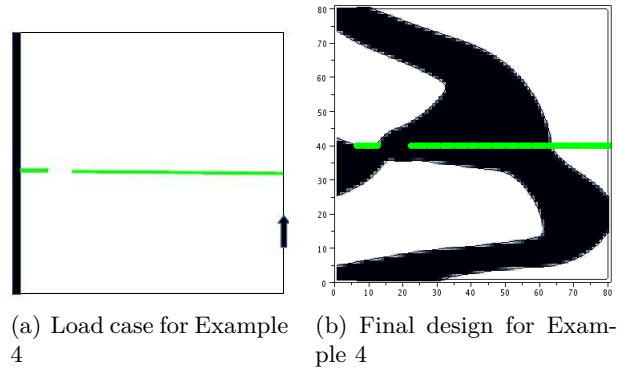


FIGURE 6.7. Example 4

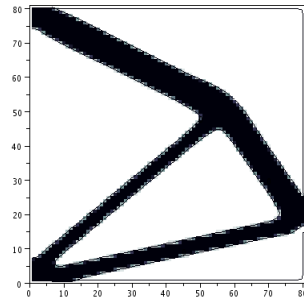


FIGURE 6.8. Final design for Example 4bis

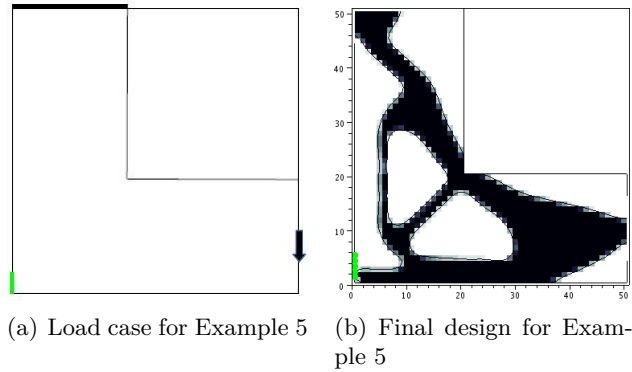


FIGURE 6.9. Example 5

solution is not admissible (its compliance is about 118). We need to weaken the compliance constraint to have a feasible starting solution for the optimisation algorithm in the case of Example 5bis.

In the next four examples (labeled from 6 to 9), the normal force criteria (4.6) and (4.7) are used to obtain different kinds of clamps or gripping mechanisms. Apart from Example 6, in which the normal force criterion is minimised under volume and compliance constraints, we minimise the volume under compliance and normal force constraints (the precise values of these constraints are given in Tables 6.3 and 6.4). The results are presented in Tables 6.3 and 6.4.

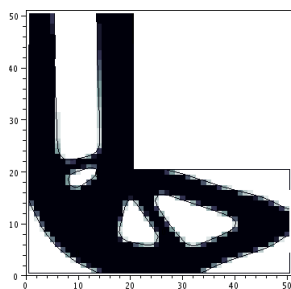


FIGURE 6.10. Final design for Example 5bis

Cases	Volume	Compliance	Compliance Constraint	Iterations	Evaluations
2	1.45211	19.9998	20	67	95
1-2bis	1.41650	19.9997	20	22	38
3	0.35078	0.499995	0.5	82	110
3bis	0.248584	0.499993	0.5	31	47
4	1.69044	29.9999	30	64	95
4bis	0.928932	29.9841	30	28	46
5	1.15278	94.9829	95	18	36
5bis	1.64209	139.906	140	18	35

TABLE 6.2. Results for sliding contact examples and Examples 1-2bis, 3bis, 4bis and 5bis.

- Example 6, here the Dirichlet conditions ( $\Gamma_0$ ) at  $(1.9, 0)$  and  $(1.9, 2)$  are put only for the  $x$  (horizontal) part of the displacement,  $\Gamma_c = \emptyset$  and two unit forces ( $\Gamma_N$ ) are applied at  $(1.8, 2)$  and  $(1.8, 0)$ . The normal force criterion used is  $l_3$  with  $c = -1.5$ . See Figure 6.11 for the results.

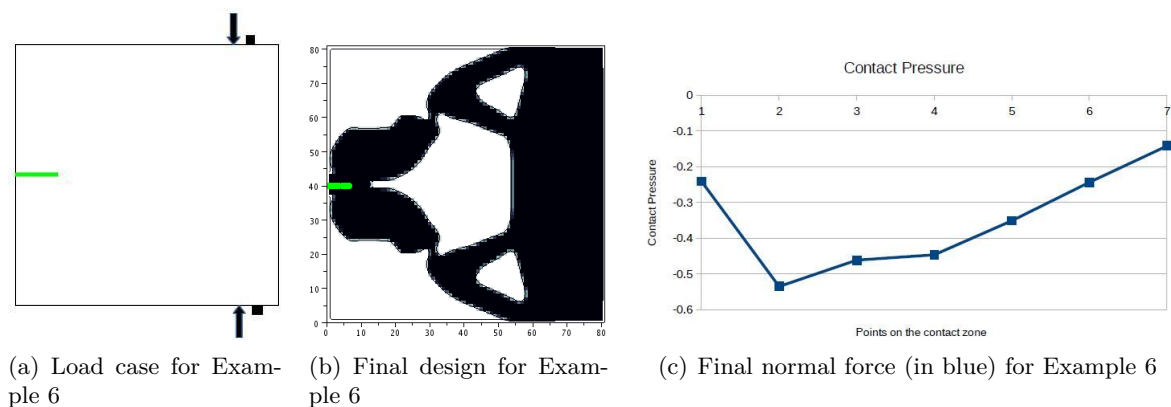


FIGURE 6.11. Example 6

The shape of a clamp is found, which manages to bring the forces from the right side to the left side, keeping their direction. We remark that we do not manage to reach the value of the threshold  $c$ . In the next example, we will use the same criterion as a constraint and see that the results are far better on this particular issue.

- Example 7, two unit forces ( $\Gamma_N$ ) are applied at  $(1.8, 2)$  and  $(1.8, 0)$ ,  $\Gamma_c = \emptyset$  and the structure is fixed ( $\Gamma_0$ ) from  $(2, 0.9)$  to  $(2, 1.1)$ . The normal force criterion used is  $l_3$  with  $c = -1.1$ . We refer to Figure 6.12 for the results.

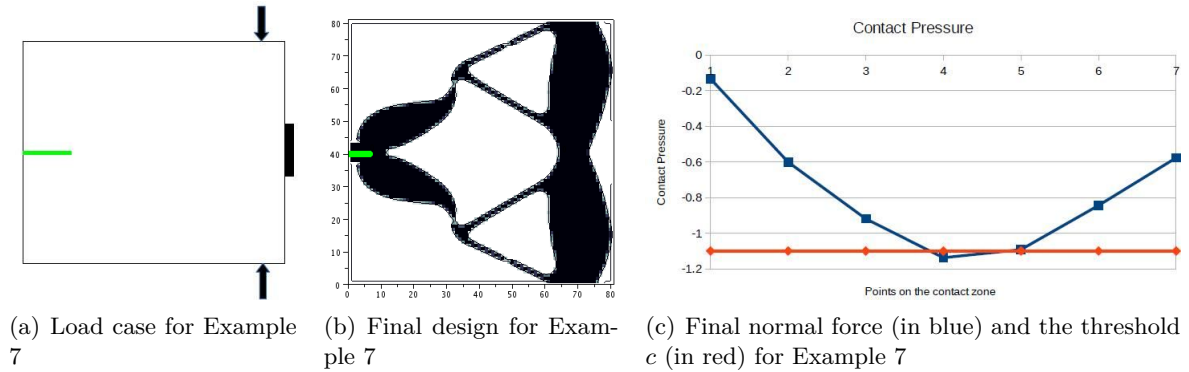


FIGURE 6.12. Example 7

The Dirichlet part on the right side is used at the beginning of the optimisation process and is finally found to be useless.

- Example 8, two unit forces ( $\Gamma_N$ ) are applied at  $(1.5, 2)$  and  $(1.5, 0)$  and  $\Gamma_c = \emptyset$ . Dirichlet conditions ( $\Gamma_0$ ) are enforced on the whole left side. The normal force criterion used is  $l_3$  with  $c = -0.9$ . Figure 6.13 presents the results.

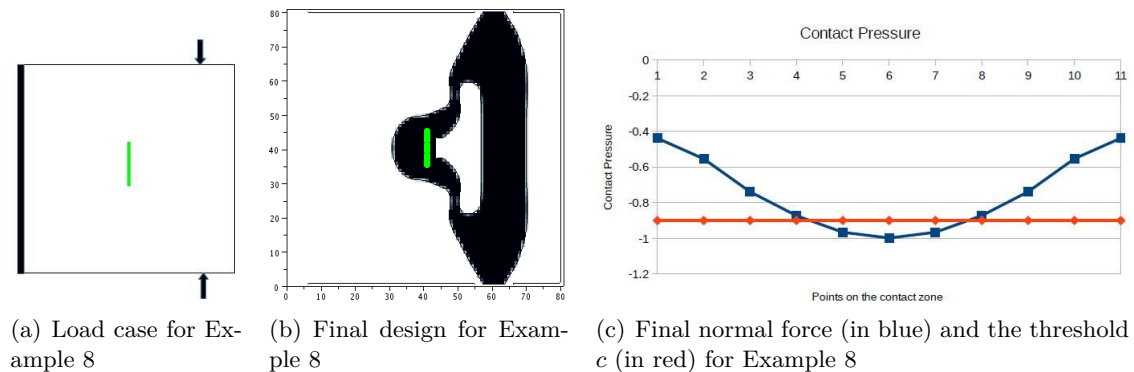


FIGURE 6.13. Example 8

On the contrary, this example shows a mechanism which transforms the vertical forces into horizontal ones.

- Example 9, the downside ( $\Gamma_0$ ) is fixed,  $\Gamma_c = \emptyset$  and two unit forces ( $\Gamma_N$ ) are applied at  $(0.2, 0)$  and  $(1.8, 0)$ . The normal force criterion used is  $l_1$  with  $c = -2$ . Figure 6.14 gives the results.

Finally Example 9 produces pillars that are perpendicular to the Dirichlet zone, linked to the contact zone by oblique bars, to distribute the force between the two zones in order to both try to reach the constraint  $l_1$  and stabilise the structure.

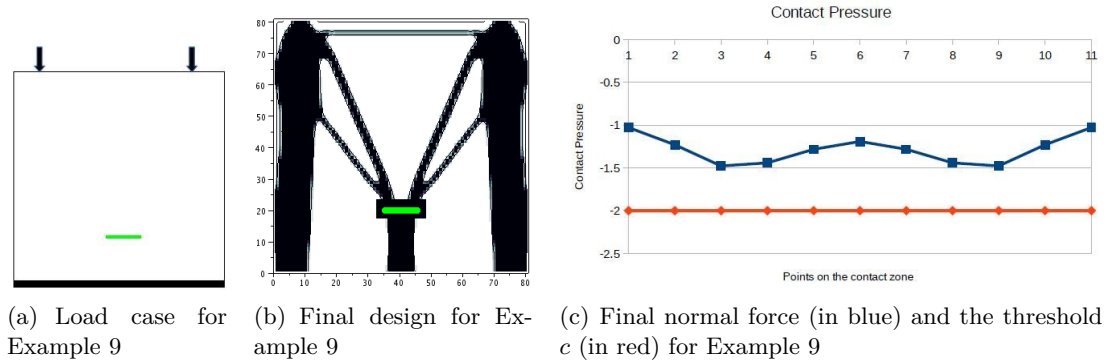


FIGURE 6.14. Example 9

Cases	Norm. force	Compl.	Compl. Constr.	Vol.	Vol. constr.	Iterations	Evaluations
6	3.03302	8.32621	8.4	2.27271	2.7	16	23

TABLE 6.3. Results for Example 6.

Cases	Vol.	Compl.	C. Constr.	Norm. force	N.f. Constr.	Iter.	Eval.
7	1.34868	10.9603	11	1.99976	2	251	275
8	0.971308	5.99801	6	1.49998	1.5	178	206
9	1.62217	14.9941	15	0.148007	0.15	24	40

TABLE 6.4. Results for Examples 7, 8 and 9

For these examples (6 to 9), it has to be noted that the computation of the normal force, thanks to the penalisation formula (4.5), is not very accurate since the displacement  $u$  is multiplied by the large penalisation factor  $1/\epsilon$ . Therefore, if one requires a precision of the order of unity for the normal force, the displacement  $u$  should be solved with a precision smaller than  $\epsilon$ , which is not the case here. Moreover, it appears that the criteria used are quite sensitive to small changes in the shape. This forbids the use of too tight normal force constraints, which explains that pointwise constraints are most of the time not exactly fulfilled. These examples are however interesting as they give a good hint of the possible optimal shape for pointwise constraints.

### 6.2.2. Contact with friction

We give four examples (labeled from 10 to 13) of contact optimisation with friction. For each of these examples, the results are displayed for all contact models: sliding (no friction), Tresca, Norton Hoff, normal compliance and Coulomb. The friction coefficient is  $\sigma_{tr}$  for the Tresca model and  $\mu$  for all other models. For the normal compliance model, we have  $C_N = 1$ ,  $m_N = 1$  and  $m_T = 1$ . For the Norton Hoff model, we recall that  $\rho$  denotes the exponent parameter defined in (2.13). We minimise the volume under a compliance constraint.

- Example 10, a unit force ( $\Gamma_N$ ) is applied at  $(2, 1)$ , the left side of the structure ( $\Gamma_0$ ) is fixed and  $\Gamma_c = \emptyset$ . The friction coefficient is 0.5 and for the Norton Hoff model  $\rho = 0.1$ . Example

10bis corresponds to the same problem without the two contact areas. Results can be found in Table 6.5 and Figures 6.15 and 6.16.

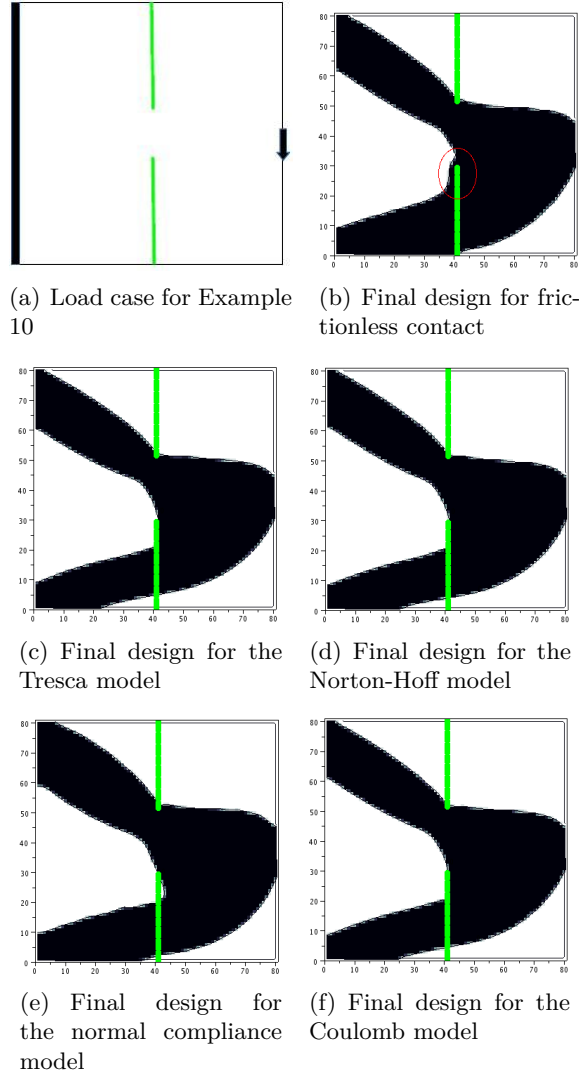


FIGURE 6.15. Example 10

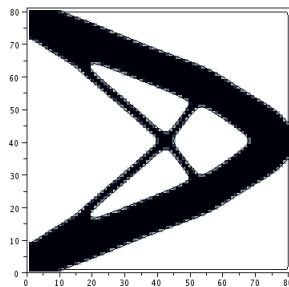


FIGURE 6.16. Final design for Example 10bis (without contact).

Cases	Volume	Compliance	Compliance Constraint	Iterations	Evaluations
Sliding contact	1.86357	19.9956	20	36	51
Tresca	1.76836	19.9999	20	47	73
Norton Hoff	1.76906	19.9999	20	41	67
Normal compliance	1.97197	19.9999	20	49	65
Coulomb	1.76948	19.9998	20	45	70
10bis	1.34787	19.9978	20	33	50

TABLE 6.5. Comparison results of friction models for Examples 10 and 10bis.

Cases	Volume	Compliance	Compliance Constraint	Iterations	Evaluations
Sliding contact	0.422235	21.9991	22	44	71
Tresca	0.302352	21.9957	22	45	71
Norton Hoff	0.309498	21.9995	22	44	65
Normal compliance	0.336178	21.9996	22	37	63
Coulomb	0.286532	21.9995	22	35	61

TABLE 6.6. Comparison results of friction models for Example 11.

Cases	Volume	Compliance	Compliance Constraint	Iterations	Evaluations
Sliding contact	0.593907	94.9994	95	22	40
Tresca	0.59725	94.9014	95	18	34
Norton Hoff	0.550918	94.5404	95	18	34
Normal compliance	0.917105	94.1346	95	13	30
Coulomb	0.907396	94.9978	95	48	67

TABLE 6.7. Comparison results of friction models for Example 12.

In all cases, the algorithm tends to avoid the upper contact zone which opens and keep the lower one. However, in sliding contact, the lower leg has to be hooked up to a part of the structure which is not in the contact zone. It is not the case in the friction cases as the friction keeps the lower leg connected to the structure (see the zone circled in red on the final design for frictionless contact and the equivalent zone on the models with friction). Example 9bis is meant to underline the impact of the contact on the optimised structure.

- Example 11, a unit force ( $\Gamma_N$ ) is applied at  $(1, 2)$  and  $S = \emptyset$ . The friction coefficient is 1.3 and for the Norton Hoff model  $\rho = 0.5$ . The results are delivered in Table 6.6 and in Figure 6.17.

In sliding contact the legs of the bridge have to be vertical to the contact zone to prevent sliding. Whereas in other cases, the friction stabilises the structure and enables the legs to incline.

- Example 12, Dirichlet conditions ( $\Gamma_0$ ) are enforced on the left up part of the L-shape,  $S = \emptyset$  and a downward unit force ( $\Gamma_N$ ) is applied at  $(2, 1.6)$ . The friction coefficient is 1.2 and for the Norton Hoff model  $\rho = 0.6$ . Results are given in Table 6.7 and Figure 6.18.

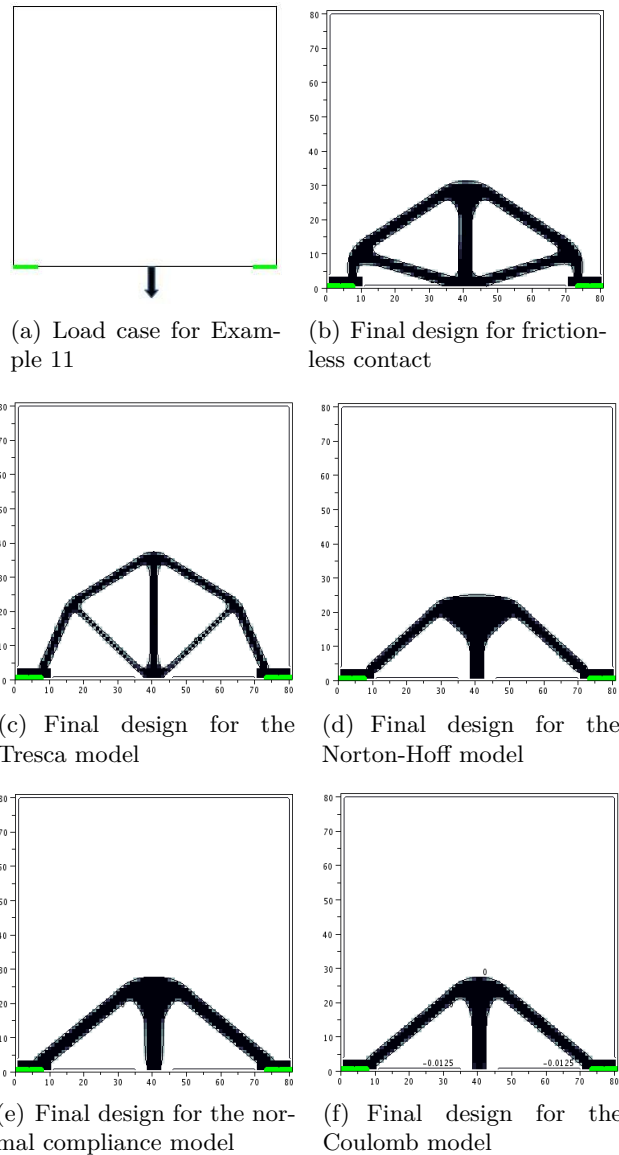


FIGURE 6.17. Example 11

The result in sliding contact can be compared with Example 5. Here the algorithm makes use of the second contact zone and, for the Norton-Hoff model, manages to use it to stabilise the structure without being connected to the Dirichlet boundary. In the case of Coulomb model, there is trouble in solving the contact problem (for several shapes, the non-linear algorithm does not converge and the displacement used for computing the shape gradients and the criteria are not accurate enough) which leads to a bad optimised result in terms of volume compared to the other models.

- Example 13, Dirichlet conditions ( $\Gamma_0$ ) are enforced from  $(1.2, 0)$  to  $(2, 0)$ ,  $S = \emptyset$  and a downward unit force ( $\Gamma_N$ ) is applied at  $(2, 1.6)$ . The friction coefficient is 0.8 and, for the Norton Hoff model,  $\rho = 0.6$ . For Example 13bis, we only remove the contact zone. Results are shown in Table 6.8 and Figures 6.19 and 6.20.

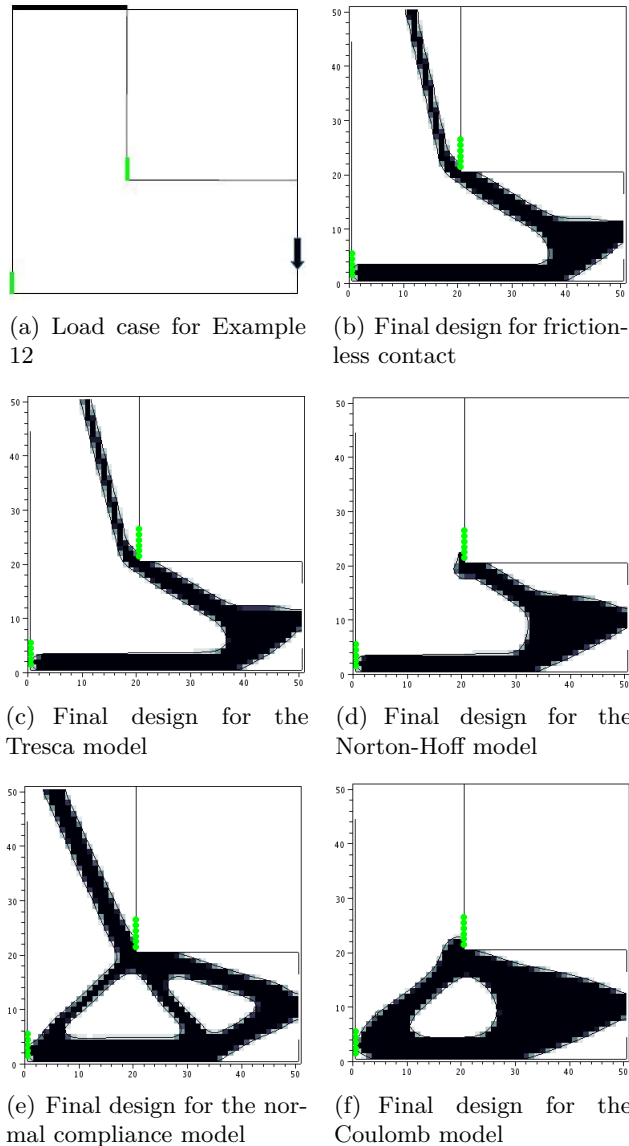


FIGURE 6.18. Example 12

The contact area enables the structure to be only connected with the Dirichlet part by its left edge and to use less material. The friction allows to slightly decrease the volume.

### 6.3. Examples in 3D

The following examples (labeled from 14 to 18) were computed thanks to the finite element software SYSTUS of ESI-Group [17]. The non-linear problems are solved thanks to a Newton algorithm. In all cases, the volume is minimised under a compliance constraint. The friction coefficient is set to 0.01. In Examples 15 to 18 we force a small amount of material to remain near the Dirichlet and force zones. In Example 14 this is done only for the force zone. To be sure that the models of sliding contact and Tresca were the same as in 2D, we choose to use node to node elements (string elements) for which we implement the penalisation adapted to the frictionless contact and the Tresca model.

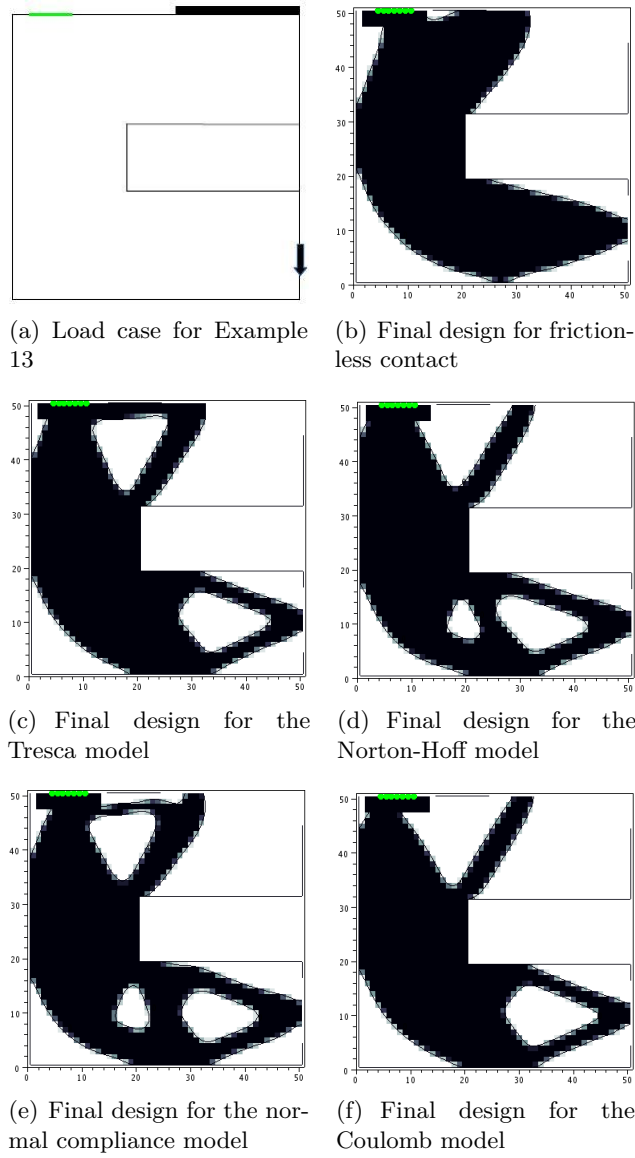


FIGURE 6.19. Example 13

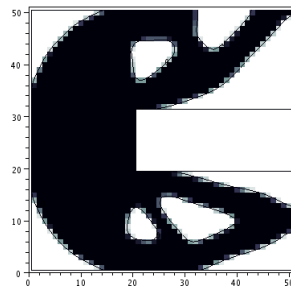


FIGURE 6.20. Final design for Example 13bis

Cases	Volume	Compliance	Compliance Constraint	Iterations	Evaluations
Sliding contact	2.15435	149.999	150	16	32
Tresca	1.95836	149.989	150	14	29
Norton Hoff	1.87089	149.881	150	25	40
Normal compliance	1.94898	149.994	150	13	28
Coulomb	1.83706	149.997	150	20	39
13bis	2.39942	149.962	150	20	36

TABLE 6.8. Comparison results of friction models for Examples 13 and 13bis.

Cases	Volume	Compliance	Compliance Constraint	Iterations	Evaluations
Sliding contact	2.521889e-01	9.994017e+03	10000	15	23
Tresca	2.555368e-01	9.999298e+03	10000	17	25

TABLE 6.9. Comparison results of friction models for Example 14.

- Example 14 features 97289 elements and 17290 nodes. A downward surface force ( $\Gamma_N$ ) equal to 10000 is applied on a square of side 0.2 in the middle of the right face. Dirichlet conditions ( $\Gamma_0$ ) are enforced on the left face (see Figure 6.21) and  $\Gamma_c = \emptyset$ . The results are gathered in Table 6.9 and in Figures 6.21, 6.22 and 6.23.

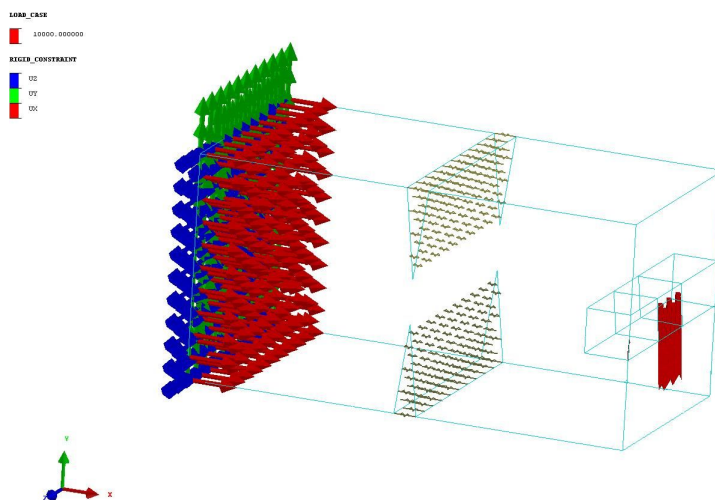


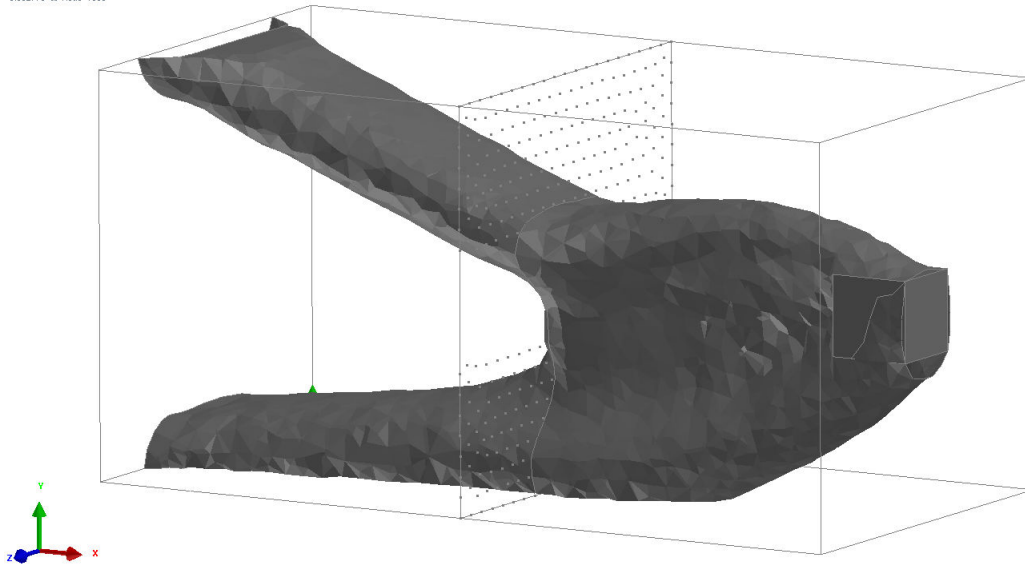
FIGURE 6.21. Load case for Example 14.

This example is the equivalent of 2D Example 10, but in 3D. We can make the same remark as in frictionless contact: the lower leg needs to be hooked up to a part of the structure not containing the contact. This is not the case when friction is possible.

- Example 15 features 156417 elements and 27312 nodes. See Table 6.10 and Figures 6.24, 6.25 and 6.26 for the results.

CANTIL SLIDING CONTACT  
 NODE = LEVELSET\_1\_NOD  
 Min = -0.115381 at Node 10355  
 Max = 0.592779 at Node 1095

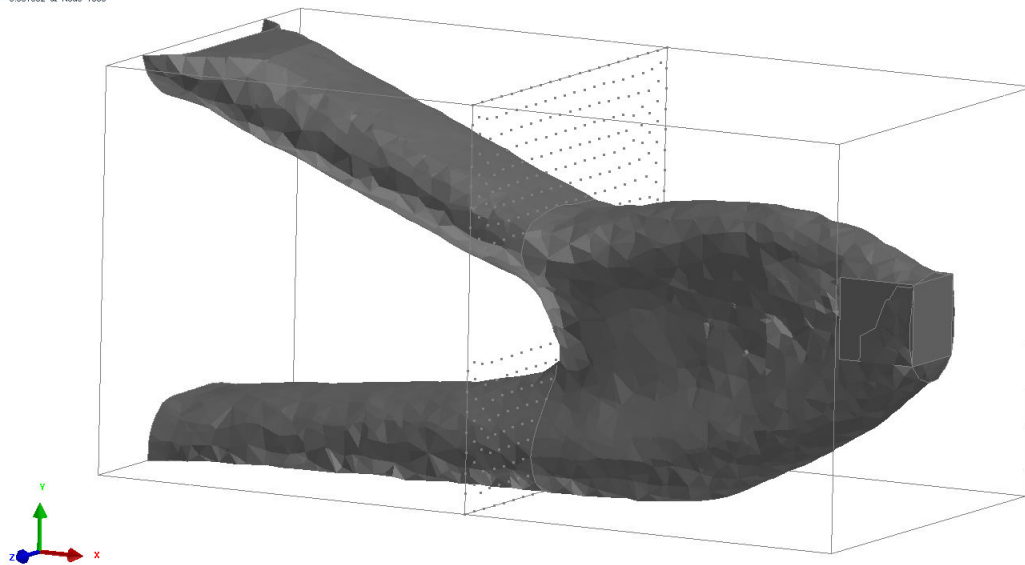
24 / 16.000700



(a) Final design for frictionless contact

CANTIL FRICTION CONTACT  
 NODE = LEVELSET\_1\_NOD  
 Min = -0.118219 at Node 10355  
 Max = 0.591992 at Node 1095

26 / 17.000799



(b) Final design for the Tresca model

FIGURE 6.22. Example 14

Here there are three circular potential contact zones ( $\Gamma_c$ ) and the forces ( $\Gamma_N$ ) are applied on two small cylinders in the middle. Two downward surface forces of 200000 magnitude are applied on a disk of radius 0.1 at the center of each circular face. Dirichlet conditions ( $\Gamma_0$ )

## SHAPE OPTIMISATION FOR CONTACT PROBLEMS

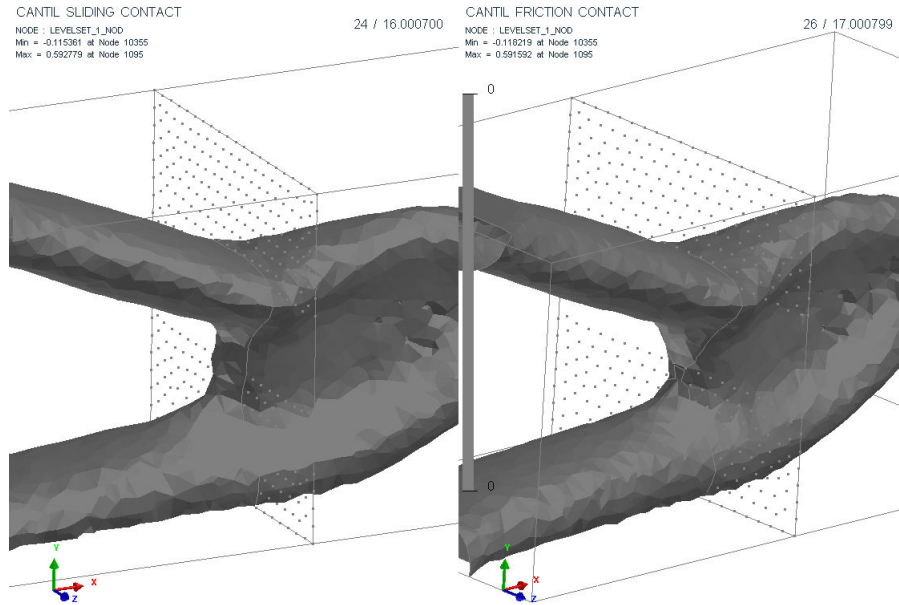


FIGURE 6.23. Comparison between the final designs without (left) and with (right) friction for Example 14. Remark the small amount of material needed only in the sliding case.

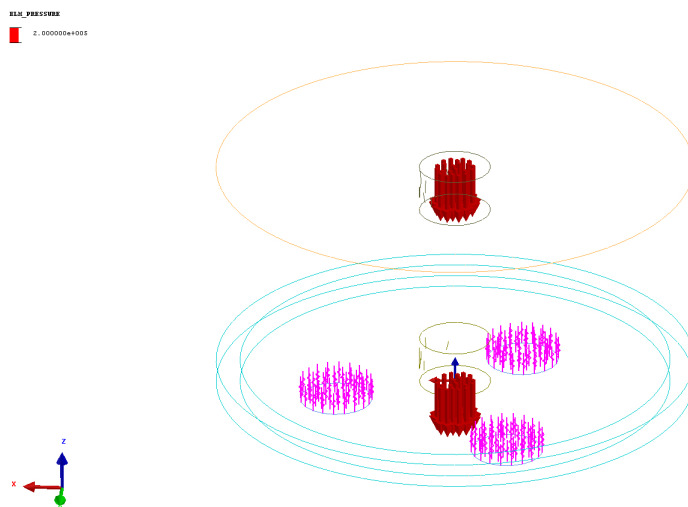


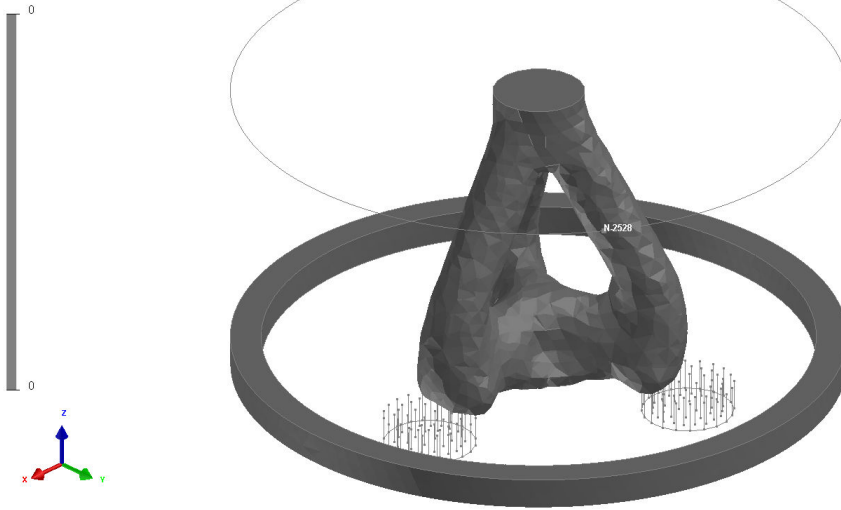
FIGURE 6.24. Load case for Example 15.

are enforced on the bottom face on a ring of length 0.1 surrounding the structure (see Figure 6.24). In both cases the contact zones are enough to stabilise the structure and the Dirichlet zone is not used. Between frictionless and friction contact, slight changes appear in the shape of the three feet of the structure.

- Example 16 features 89475 elements and 15895 nodes. Table 6.11 and Figures 6.27 and 6.28 show the results.

BRIDGE SLIDING CONTACT  
 NODE : LEVELSET\_1\_INDO  
 Min = -0.138236 at Node 5244  
 Max = 0.068504 at Node 2528

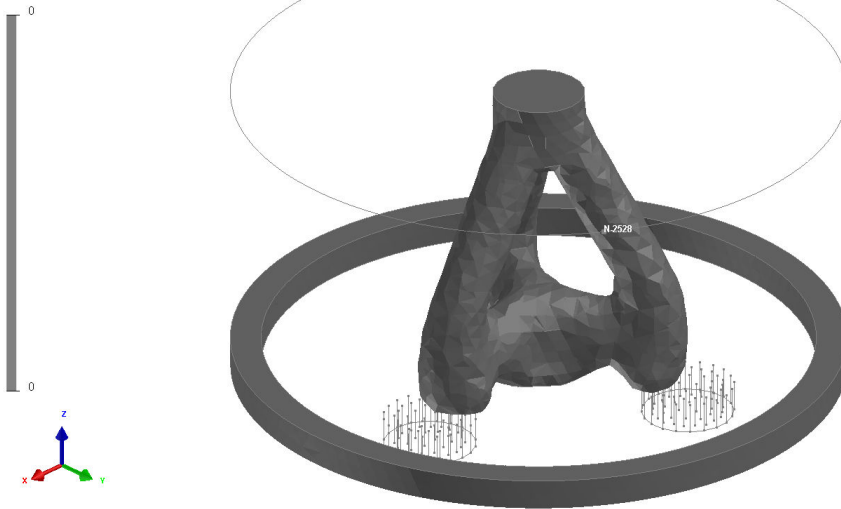
41 / 30.000999



(a) Final design for frictionless contact

CYLINDER SLIDING CONTACT  
 NODE : LEVELSET\_1\_INDO  
 Min = -0.132872 at Node 5244  
 Max = 0.068913 at Node 2528

46 / 36.000900



(b) Final design for the Tresca model

FIGURE 6.25. Example 15

The cylinder in the center and the bottom left side ( $\Gamma_0$ ) are completely fixed and  $S = \emptyset$ . A downward 50000 force ( $\Gamma_N$ ) is applied on a rectangular part of the bottom face of dimension  $0.1 \times 1$  on the far right (see Figure 6.27). As the cylinder in the center is fixed, the algorithm uses it to stabilise the structure. In the frictionless case it needs to turn around the cylinder as sliding is possible. In the friction case this is not needed anymore, but we remark that a small part of matter remains under the cylinder, going to it from the base. This part is not

## SHAPE OPTIMISATION FOR CONTACT PROBLEMS

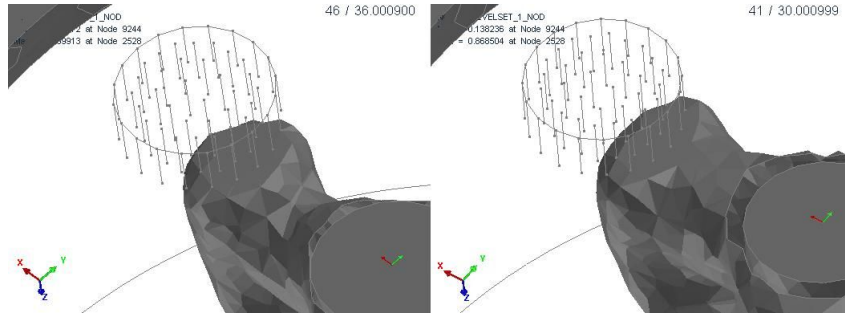


FIGURE 6.26. Comparison between the final designs without (left) and with (right) friction for Example 15. Remark that the shape of the foot is larger when friction is present.

Cases	Volume	Compliance	Compliance Constraint	Iterations	Evaluations
Sliding contact	2.078838e-01	9.987082e+03	10000	29	40
Tresca	1.920865e-01	9.987843e+03	10000	36	45

TABLE 6.10. Comparison results of friction models for Example 15.

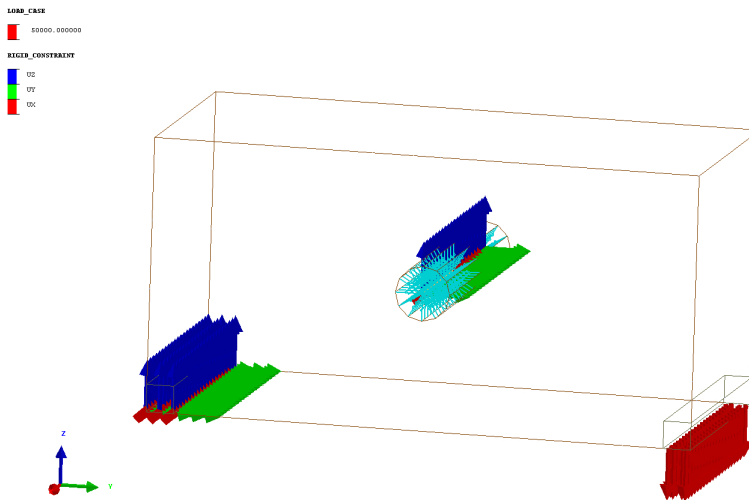
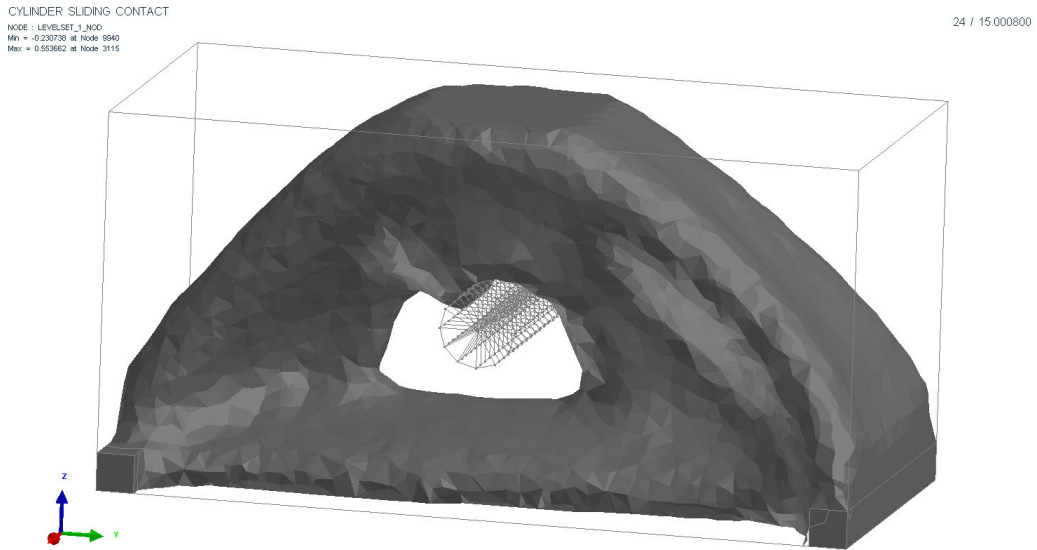


FIGURE 6.27. Load case for Example 16.

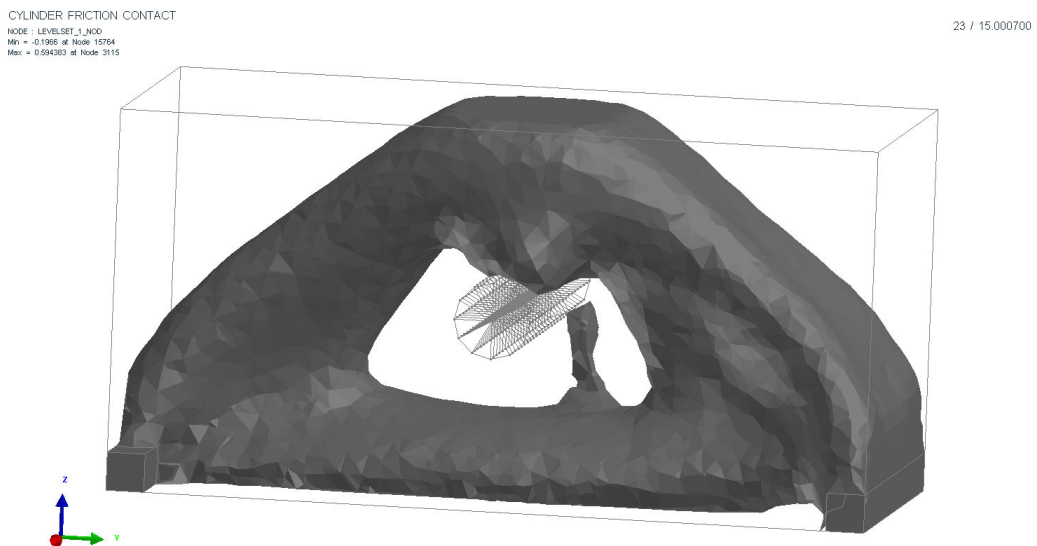
Cases	Volume	Compliance	Compliance Constraint	Iterations	Evaluations
Sliding contact	7.082515e-01	9.990895e+03	10000	14	23
Tresca	6.915364e-01	9.979266e+03	10000	14	22

TABLE 6.11. Comparison results of friction models for Example 16.

in contact but the tangential displacements are such that friction occurs (which is one of the problems of the Tresca model making it non-mechanically correct).



(a) Final design for frictionless contact



(b) Final design for the Tresca model

FIGURE 6.28. Example 16

- Example 17 features 89475 elements and 15895 nodes. Table 6.12 and Figures 6.29, 6.30 and 6.31 gather the results.

A downward force ( $\Gamma_N$ ) of 50000 magnitude is applied on the whole cylinder axis and on the left and right bottom parts, a rectangular part of dimension  $0.1 \times 1$  ( $\Gamma_0$ ) is fixed and  $S = \emptyset$ . The cylinder is encircled by matter to be supported (see Figure 6.29). The differences between the sliding and the friction case come from the fact that in the friction case the optimisation algorithm stopped prematurely due to convergence problems in the contact solver.

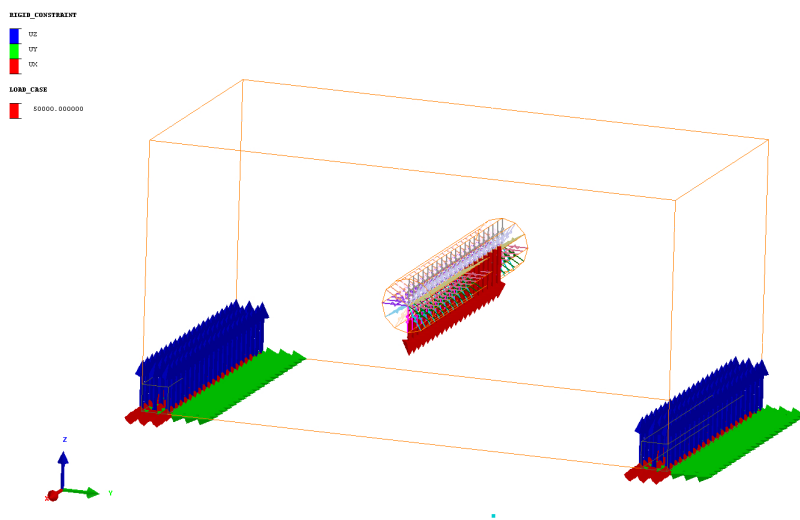


FIGURE 6.29. Load case for Example 17.

Cases	Volume	Compliance	Compliance Constraint	Iterations	Evaluations
Sliding contact	3.293794e-01	9.997417e+03	10000	78	87
Tresca	3.322390e-01	9.860692e+03	10000	22	33

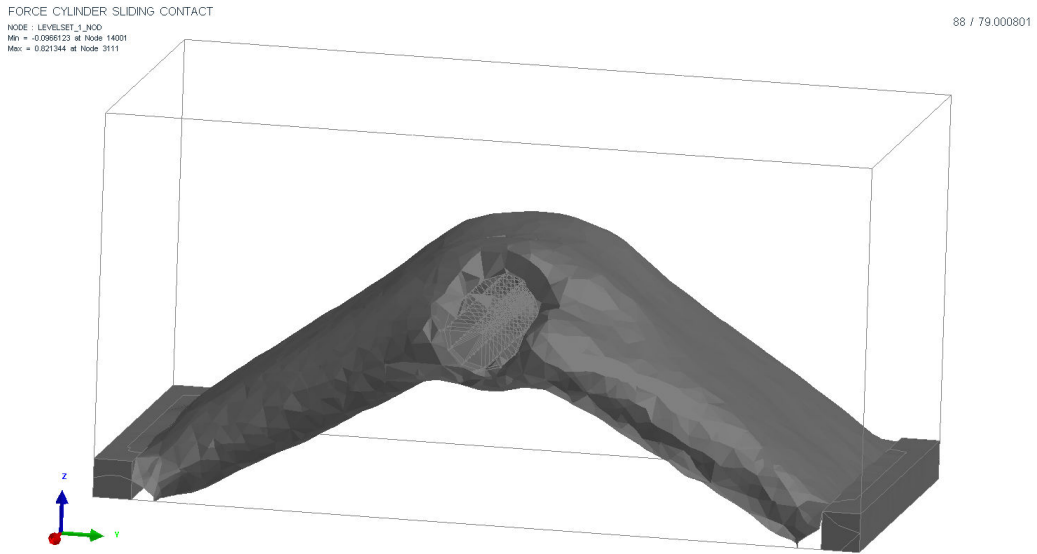
TABLE 6.12. Comparison results of friction models for Example 17.

Cases	Volume	Compliance	Compliance Constraint	Iterations	Evaluations
Sliding contact	2.349350e-01	1.981722e+04	20000	81	89
Tresca	2.299134e-01	1.986286e+04	10000	100	111

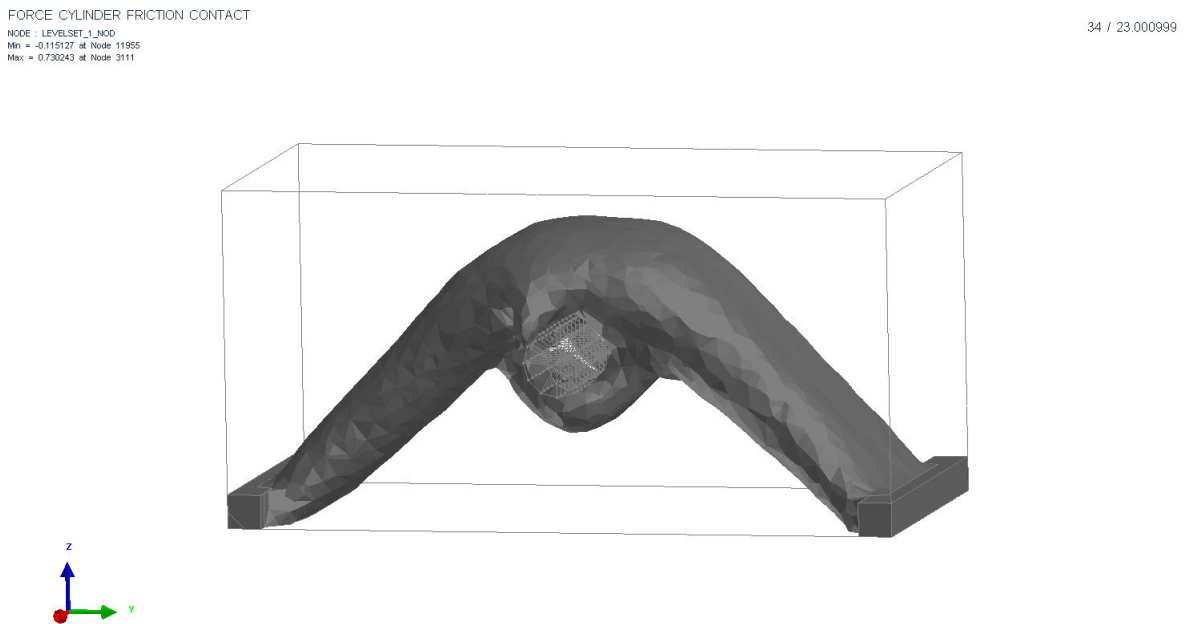
TABLE 6.13. Comparison results of friction models for Example 18.

- Example 18 features 90205 elements and 16010 nodes. Table 6.13 and Figures 6.32 and 6.33 present the results.

The cylinder ( $\Gamma_0$ ) is fixed only in the  $y$  and  $x$  directions and  $S = \emptyset$ . A downward force ( $\Gamma_N$ ) of 20000 magnitude is applied on the whole cylinder axis and two downward forces ( $\Gamma_N$ ) of 50000 magnitude are applied on two rectangular parts of the downside face of dimension  $0.1 \times 1$  on the far right and the far left. Finally we fix two parts on the bottom ( $\Gamma_0$ ). The structure only needs to support the cylinder and the forces on the left and right side (see Figure 6.32 for details). To perform that, it uses archways in order to lead to the middle of the structure forces on the sides, changing their direction in the opposite one and, this way, using them to support the force of the cylinder. Due to the Dirichlet conditions put on the cylinder, the fact that the results are the same with or without friction is not a surprise.



(a) Final design for frictionless contact



(b) Final design for the Tresca model

FIGURE 6.30. Example 17

## 7. Conclusion

Through all the numerical examples shown in this article, the regularised and penalised formulations are proved to be good ways to cope with the non-differentiability of problems having a unique solution. Despite the possible non-uniqueness of its solution, the Norton Hoff model behaves well in this

## SHAPE OPTIMISATION FOR CONTACT PROBLEMS

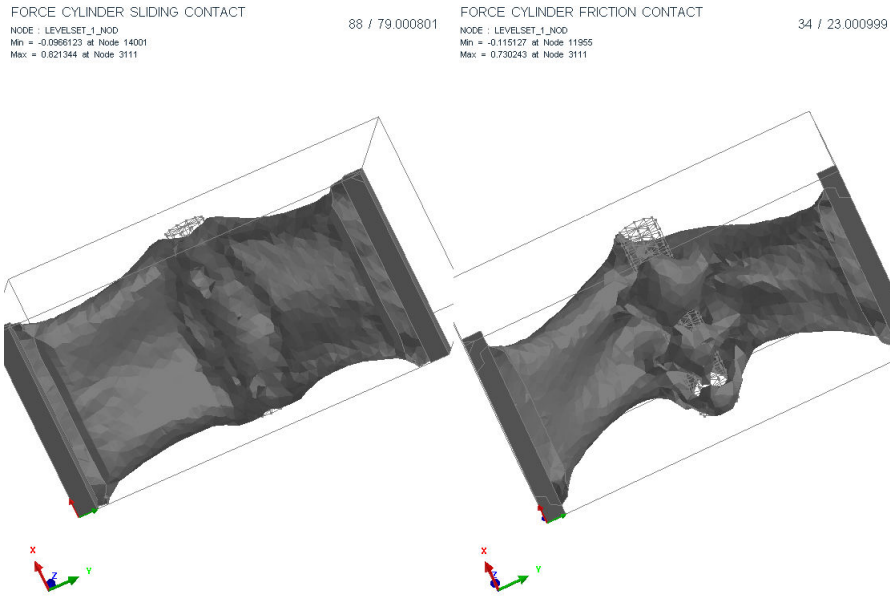


FIGURE 6.31. Comparison between the final designs without (left) and with (right) friction viewed from below for Example 17

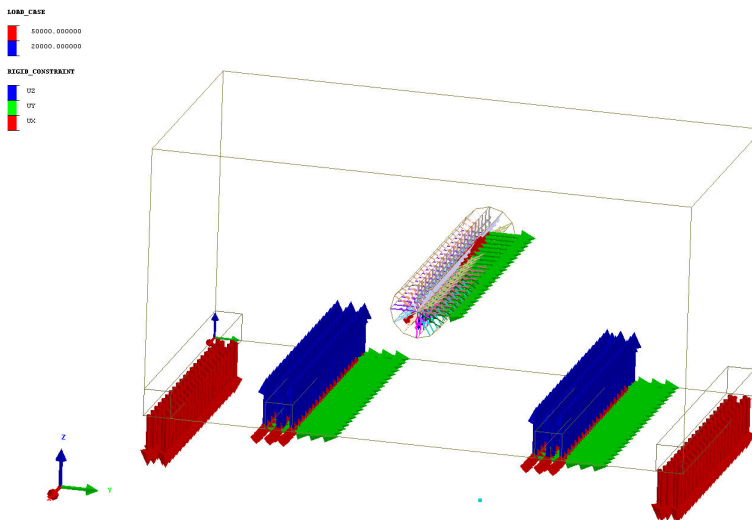


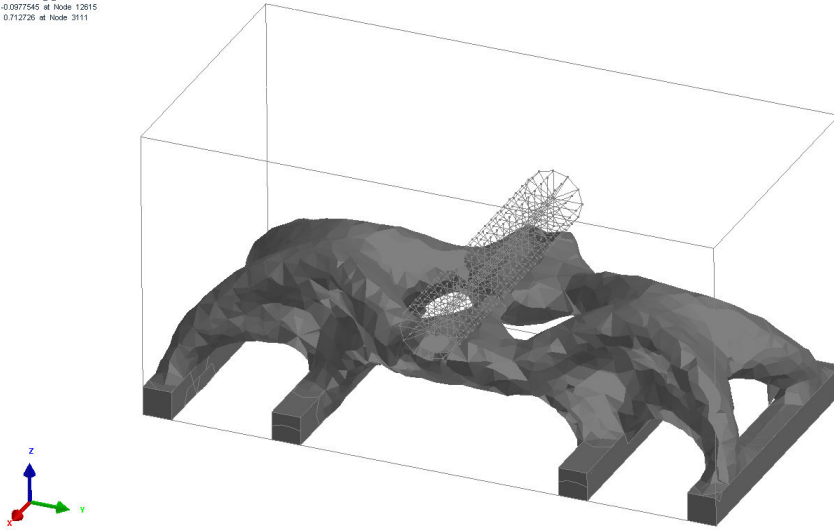
FIGURE 6.32. Load case for Example 18.

framework. On the contrary, the Coulomb model presents some difficulties due to a bad convergence in the contact solver. It then appears that the crucial point is the robustness of the contact solver which has to converge in every situation for the optimisation process to succeed. In 3D we used a Newton method to solve the contact problem. It is a good practice (compared to a fixed point algorithm) since it furnishes the tangent matrix  $M$  which is precisely the transpose of the stiffness matrix for the adjoint problem. This was of great help for our implementation in the ESI group software.

Concerning the criteria depending on the normal force, we have to be cautious with our numerical results, as the approximations made (finite element method with penalisation) may not allow a

FORCE CYLINDER SLIDING CONTACT  
 NODE : LEVELSET\_1\_200  
 Min = -0.997545 at Node 12615  
 Max = 0.712726 at Node 3111

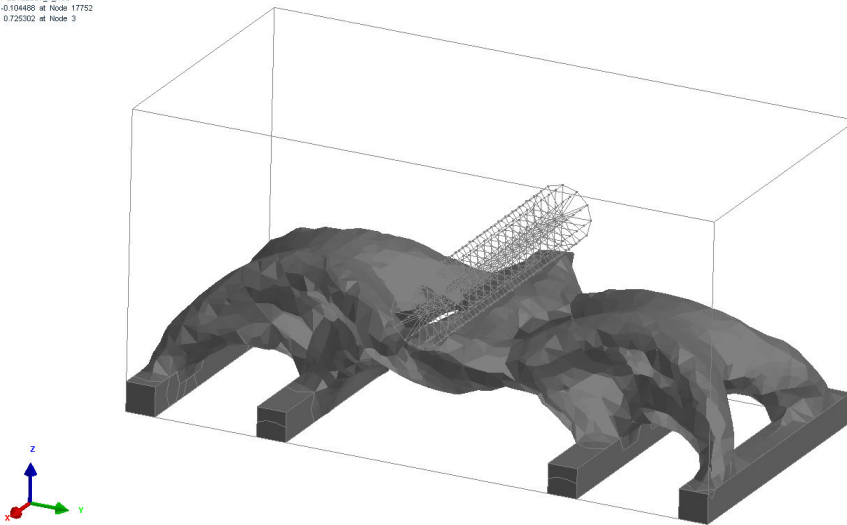
90 / 81.000801



(a) Final design for frictionless contact

FORCE CYLINDER FRICTION CONTACT  
 NODE : LEVELSET\_1\_200  
 Min = -0.104488 at Node 17752  
 Max = 0.725302 at Node 3

112 / 100.001099



(b) Final design for the Tresca model

FIGURE 6.33. Example 18

sufficient accuracy on the computed force. However, these criteria can be used to create compliant mechanisms such as in Examples 6, 7 and 8 or in [43], or, as in Example 8, to get a shape which tends to uniformise the normal force.

To go one step beyond our approach, we could eliminate the regularisation and work in the context of non-smooth optimisation. In such a case, one has to use subgradients algorithms. Subgradients were computed for the problems written as variational inequalities in [33] and [51]. It yields a better accuracy on the normal force and gives good results for optimisation with Coulomb friction [7]. Note

that [7], [33] and [51], focus on the optimisation of the discrete problem. Finally contact time-dependent problems could also be studied.

**Acknowledgements.** This work has been supported by the RODIN project (FUI AAP 13). The second author G. Allaire is a member of the DEFI project at INRIA Saclay Ile-de-France. The authors acknowledge the help of Philippe Conraux and Damien Lachouette (ESI group) for the computations performed with the SYSTUS code.

## References

- [1] G. Allaire. *Conception optimale de structures*, volume 58 of *Mathématiques & Applications [Mathematics & Applications]*. Springer-Verlag, Berlin, 2007.
- [2] G. Allaire, F. Jouve, and A.-M. Toader. Structural optimization using sensitivity analysis and a level-set method. *Journal of computational physics*, 194(1):363–393, 2004.
- [3] A. Amassad, D. Chenaïs, and C. Fabre. Optimal control of an elastic contact problem involving Tresca friction law. *Nonlinear Anal.*, 48(8, Ser. A: Theory Methods):1107–1135, 2002.
- [4] J. Andersson. Optimal regularity and free boundary regularity for the Signorini problem. *Algebra i Analiz*, 24(3):1–21, 2012.
- [5] J. Andersson. Optimal regularity for the Signorini problem and its free boundary. *Invent. Math.*, 204(1):1–82, 2016.
- [6] V. Barbu. *Optimal control of variational inequalities*, volume 100 of *Research Notes in Mathematics*. Pitman (Advanced Publishing Program), Boston, MA, 1984.
- [7] P. Beremlijski, J. Haslinger, M. Kočvara, and J.V. Outrata. Shape optimization in contact problems with Coulomb friction. *SIAM J. Optim.*, 13(2):561–587, 2002.
- [8] P. Beremlijski, J. Haslinger, J.V. Outrata, and R. Pathó. Shape optimization in contact problems with Coulomb friction and a solution-dependent friction coefficient. *SIAM J. Control Optim.*, 52(5):3371–3400, 2014.
- [9] P. Boieri, F. Gastaldi, and D. Kinderlehrer. Existence, uniqueness, and regularity results for the two-body contact problem. *Appl. Math. Optim.*, 15(3):251–277, 1987.
- [10] J. Cea. Conception optimale ou identification de formes: calcul rapide de la dérivée directionnelle de la fonction coût. *RAIRO Modél. Math. Anal. Numér.*, 20(3):371–402, 1986.
- [11] W.-H. Chen and C.-R. Ou. Shape optimization in contact problems with desired contact traction distribution on the specified contact surface. *Computational Mechanics*, 15:534–545, 1995.
- [12] J.E. Jr. Dennis and R.B. Schnabel. *Numerical methods for unconstrained optimization and nonlinear equations*, volume 16 of *Classics in Applied Mathematics*. Society for Industrial and Applied Mathematics (SIAM), Philadelphia, PA, 1996. Corrected reprint of the 1983 original.
- [13] B. Desmorat. Structural rigidity optimization with frictionless unilateral contact. *Internat. J. Solids Structures*, 44(3-4):1132–1144, 2007.
- [14] S. Drabla, M. Sofonea, and B. Teniou. Analysis of a frictionless contact problem for elastic bodies. *Ann. Polon. Math.*, 69(1):75–88, 1998.
- [15] G. Duvaut and J.L. Lions. *Les inéquations en mécanique et en physique*, volume 21 of *Travaux et Recherches Mathématiques*. Dunod, Paris, 1972.
- [16] C. Eck, J. Jarusek, and M. Krbec. *Unilateral contact problems, Variational methods and existence theorems*, volume 270 of *Pure and Applied Mathematics (Boca Raton)*. Chapman & Hall/CRC, Boca Raton, FL, 2005.
- [17] ESI-group. *SYSTUS: a multiphysics simulation software*.

- [18] R. Glowinski, J.L. Lions, and R. Trémolières. *Analyse numérique des inéquations variationnelles. Tome 1, Théorie générale premières applications*, volume 5 of *Méthodes Mathématiques de l'Informatique*. Dunod, Paris, 1976.
- [19] H. Goldberg, W. Kampowsky, and F. Tröltzsch. On Nemytskij operators in  $L_p$ -spaces of abstract functions. *Math. Nachr.*, 155:127–140, 1992.
- [20] W. Han. On the numerical approximation of a frictional contact problem with normal compliance. *Numer. Funct. Anal. Optim.*, 17(3-4):307–321, 1996.
- [21] J. Haslinger. Approximation of the Signorini problem with friction, obeying the Coulomb law. *Math. Methods Appl. Sci.*, 5(3):422–437, 1983.
- [22] J. Haslinger. Shape optimization in contact problems. In *Equadiff 6 (Brno, 1985)*, pages 445–450. Univ. J. E. Purkyně, Brno, 1986.
- [23] J. Haslinger. Signorini problem with Coulomb's law of friction. Shape optimization in contact problems. *Internat. J. Numer. Methods Engrg.*, 34(1):223–231, 1992. The Second World Congress of Computational Mechanics, Part I (Stuttgart, 1990).
- [24] J. Haslinger and A. Klarbring. Shape optimization in unilateral contact problems using generalized reciprocal energy as objective functional. *Nonlinear Anal.*, 21(11):815–834, 1993.
- [25] J. Haslinger and P. Neittaanmäki. On the existence of optimal shapes in contact problems. *Numer. Funct. Anal. Optim.*, 7(2-3):107–124, 1984/85.
- [26] J. Haslinger and P. Neittaanmäki. Shape optimization in contact problems. Approximation and numerical realization. *RAIRO Modél. Math. Anal. Numér.*, 21(2):269–291, 1987.
- [27] J. Haslinger, P. Neittaanmäki, and T. Tiihonen. Shape optimization in contact problems based on penalization of the state inequality. *Apl. Mat.*, 31(1):54–77, 1986.
- [28] A. Henrot and M. Pierre. *Variation et optimisation de formes, une analyse géométrique. [A geometric analysis]*, volume 48 of *Mathématiques & Applications [Mathematics & Applications]*. Springer, Berlin, 2005.
- [29] J Herskovits, A Leontiev, G Dias, and G Santos. Contact shape optimization: a bilevel programming approach. *Structural and multidisciplinary optimization*, 20(3):214–221, 2000.
- [30] P. Hild. Two results on solution uniqueness and multiplicity for the linear elastic friction problem with normal compliance. *Nonlinear Anal.*, 71(11):5560–5571, 2009.
- [31] D. Hilding, A. Klarbring, and J. Petersson. Optimization of structures in unilateral contact. *ASME Appl Mech Rev*, 52(4):1–4, 1999.
- [32] T. Iwai, A. Sugimoto, T. Aoyama, and H. Azegami. Shape optimization problem of elastic bodies for controlling contact pressure. *JSIAM Lett.*, 2:1–4, 2010.
- [33] J. Jarušek and J.V. Outrata. On sharp necessary optimality conditions in control of contact problems with strings. *Nonlinear Anal.*, 67(4):1117–1128, 2007.
- [34] N.H. Kim, K.K. Choi, and J.S. Chen. Shape design sensitivity analysis and optimization of elasto-plasticity with frictional contact. *AIAA Journal*, 38(9):1742–1753, 2000.
- [35] N.H. Kim, K.K. Choi, J.S. Chen, and Y.H. Park. Meshless shape design sensitivity analysis and optimization for contact problem with friction. *Computational Mechanics*, 25:157–168, 2000.
- [36] D. Kinderlehrer and G. Stampacchia. *An introduction to variational inequalities and their applications*, volume 88 of *Pure and Applied Mathematics*. Academic Press, Inc. [Harcourt Brace Jovanovich, Publishers], New York-London, 1980.
- [37] A. Klarbring. On the problem of optimizing contact force distributions. *J. Optim. Theory Appl.*, 74(1):131–150, 1992.

- [38] A. Klarbring, A. Mikelić, and M. Shillor. On friction problems with normal compliance. *Nonlinear Anal.*, 13(8):935–955, 1989.
- [39] A. Klarbring, A. Mikelić, and M. Shillor. Optimal shape design in contact problems with normal compliance and friction. *Appl. Math. Lett.*, 5(2):51–55, 1992.
- [40] D. Knees and A. Schröder. Global spatial regularity for elasticity models with cracks, contact and other nonsmooth constraints. *Math. Methods Appl. Sci.*, 35(15):1859–1884, 2012.
- [41] P. Laborde and Y. Renard. Fixed point strategies for elastostatic frictional contact problems. *Math. Methods Appl. Sci.*, 31(4):415–441, 2008.
- [42] W. Li, Q. Li, G. P. Steven, and Y.M. Xie. An evolutionary shape optimization for elastic contact problems subject to multiple load cases. *Computer methods in applied mechanics and engineering*, 194(30):3394–3415, 2005.
- [43] N.D. Mankame and G.K. Ananthasuresh. Topology optimization for synthesis of contact-aided compliant mechanisms using regularized contact modeling. *International Conference on Modeling, Simulation and Optimization for Design of Multi-disciplinary Engineering Systems 24-26 September, Goa, India*, 2004.
- [44] F. Mignot. Contrôle dans les inéquations variationnelles elliptiques. *Journal of Functional Analysis*, 22(2):130–185, 1976.
- [45] I. Milne, R.O. Ritchie, and B. Karihaloo. *Comprehensive structural integrity*. Elsevier Science, 2003.
- [46] F. Murat and J. Simon. Etudes de problèmes d’optimal design. *Lecture Notes in Computer Science, Springer Verlag, Berlin*, 41:54–62, 1976.
- [47] J. T. Oden and J. A. C. Martins. Models and computational methods for dynamic friction phenomena. *Comput. Methods Appl. Mech. Engrg.*, 52(1-3):527–634, 1985. FENOMECH ’84, Part III, IV (Stuttgart, 1984).
- [48] S. Osher and R. Fedkiw. *Level set methods and dynamic implicit surfaces*, volume 153 of *Applied Mathematical Sciences*. Springer-Verlag, New York, 2003.
- [49] S. Osher and J.A. Sethian. Fronts propagating with curvature-dependent speed: algorithms based on Hamilton-Jacobi formulations. *J. Comput. Phys.*, 79(1):12–49, 1988.
- [50] J.V. Outrata. On the numerical solution of a class of Stackelberg problems. *Z. Oper. Res.*, 34(4):255–277, 1990.
- [51] J.V. Outrata, J. Jarušek, and J. Stará. On optimality conditions in control of elliptic variational inequalities. *Set-Valued Var. Anal.*, 19(1):23–42, 2011.
- [52] I. Paczelt and T. Szabo. Optimal shape design for contact problems. *Structural Optimization*, 7:66–75, 1994.
- [53] O. Pironneau. *Optimal shape design for elliptic systems*. Springer Series in Computational Physics. Springer-Verlag, New York, 1984.
- [54] R. Schumann. Regularity for Signorini’s problem in linear elasticity. *Manuscripta Math.*, 63:255–291, 1989.
- [55] Scilab Enterprises. *Scilab: Le logiciel open source gratuit de calcul numérique*. Scilab Enterprises, Orsay, France, 2012.
- [56] J.A. Sethian. *Level set methods and fast marching methods, Evolving interfaces in computational geometry, fluid mechanics, computer vision, and materials science*, volume 3 of *Cambridge Monographs on Applied and Computational Mathematics*. Cambridge University Press, Cambridge, second edition, 1999.
- [57] J. Simon. Differentiation with respect to the domain in boundary value problems. *Numer. Funct. Anal. Optim.*, 2(7-8):649–687 (1981), 1980.
- [58] J. Sokolowski and J-P. Zolesio. *Introduction to shape optimization, shape sensitivity analysis*, volume 16 of *Springer Series in Computational Mathematics*. Springer-Verlag, Berlin, 1992.

- [59] N. Strömberg and A. Klarbring. Topology optimization of structures with contact constraints by using a smooth formulation and a nested approach. *8th World Congress on Structural and Multidisciplinary Optimization*, 2009.
- [60] N. Strömberg and A. Klarbring. Topology optimization of structures in unilateral contact. *Struct. Multidiscip. Optim.*, 41(1):57–64, 2010.
- [61] S. Stupkiewicz, J. Lengiewicz, and J. Korelc. Sensitivity analysis for frictional contact problems in the augmented Lagrangian formulation. *Comput. Methods Appl. Mech. Engrg.*, 199(33-36):2165–2176, 2010.
- [62] N. Tardieu and A. Constantinescu. On the determination of elastic coefficients from indentation experiments. *Inverse Problems*, 16(3):577–588, 2000.
- [63] F. Tröltzsch. *Optimal control of partial differential equations, Theory, methods and applications*, volume 112 of *Graduate Studies in Mathematics*. American Mathematical Society, Providence, RI, 2010.
- [64] M.Y. Wang, X. Wang, and D. Guo. A level set method for structural topology optimization. *Comput. Methods Appl. Mech. Engrg.*, 192(1-2):227–246, 2003.